# Settling Behaviors of Microplastic Disks in the Acceleration and Terminal Processes in Stagnant Water

by

Ge Yang

A thesis submitted in partial fulfillment of the requirements for the degree of

Master of Science

in

Water Resources Engineering

Department of Civil and Environmental Engineering

University of Alberta

**ABSTRACT**

The amount of plastic production grows since the 1950s. Due to poor management and high durability of plastics, they enter and accumulate in the environment. Microplastics (MPs) defined as small (< 5 mm) plastic particles have been widely found in aquatic environments, which threaten biotas and the environment. Although MPs become one of the global major concerns, hydrodynamic properties of MPs are still poorly understood. In oceans, MPs predominantly accumulate on the seafloor, indicating the importance of MP settling process. So far, settling process of microplastic (MP) disks have not been reported, which is the focus of this MSc thesis.

In this thesis, systematic experiments were conducted on MP disk settling processes with three shapes (square, rectangle and triangle) and four common-used plastic materials (ABS, PC, PET and PVC with densities of 1.038 - 1.343 g/cm$^3$). The thesis mainly includes two parts: Part I "*Terminal Settling of Microplastic Disks in Stagnant Water*"; and Part II "*Acceleration Fall of Microplastic Disks in Stagnant Water*". Part I and Part II examine MP settling behaviors after and before reaching their terminal settling velocity, respectively.

In Part I, during the terminal settling process, lighter MP disks (with density $\rho_s$ = 1.038 g/cm$^3$ and length $l \leq 5$ mm) followed rectilinear vertical trajectories, while heavier MP disks ($\rho_s$ = 1.161 - 1.343 g/cm$^3$ and $l$ = 5 mm) followed zigzag trajectories with oscillations and rotations. The mean terminal settling velocities of MP disks were 19.6 - 48.8 mm/s. Instantaneous settling velocities of heavier MP disks fluctuated. Existing formulas could not accurately predict the settling velocity of MP disks; and thus, a new model was proposed with an error of 15.5%. The

$Re_d$ - $I^*$ diagram ($Re_d$ is the disk Reynolds number and $I^*$ is the dimensionless moment of inertia) was extended for MP disks to predict settling trajectories.

In Part II, the initial acceleration process of MP disks was investigated from the point of release and before they reach the terminal settling velocities. In fact, this process has not been studied for any MP particles (not just MP disks). MP disks were released in stagnant water in five ways (different sides of MP disks facing downward) and three angles (0° - horizontal, 45°, and 90° - vertical). It was found that the MP disks with release angles of 0° start to zigzag immediately after release, while the MP disks with release angles of 45° and 90° experience an adjustment phase first where they adjust to the horizontal position before zigzagging. The adjustment distances in the vertical ($L_x$) and horizontal ($L_y$) directions, as well as the maximum vertical settling velocity ($W_{x,max}$), are influenced by the density, size, release angle and release way of MP disks. The detailed instantaneous settling trajectory and velocity were analyzed, and the relationships for predicting $L_x$, $L_y$ and $W_{x,max}$ were proposed. The drag coefficient of MP disks in the acceleration process, which changes with time, was also examined and discussed.

Finally, general conclusions and future work directions were provided at the end of the thesis.

## PREFACE

The thesis is original work by Ge Yang under the supervision of Dr. Wenming Zhang. The laboratory experiments in Chapter 2 and Chapter 3 are designed and conducted by myself. The data analysis and all of the other parts of the thesis are my original work with the assistance of Dr. Zhang,

The content of Chapter 2 has been submitted as a journal paper:

- Yang, G., Yu, Z., Baki, A.B., Yao, W., Ross, M., & Zhang, W. (2022) “Settling Behaviors of Microplastic Disks in Water”, *Marine Pollution Bulletin* (Manuscript submitted for publication).

Chapter 3 is currently being prepared as a journal manuscript.

**ACKNOWLEDGEMENTS**

This project would not be possible to finish without the help and support of many people. I would express my thanks to them.

Many thanks to my supervisor Dr. Wenming Zhang, who has been an ideal mentor and supervisor. I really appreciate his help, guidance and encouragement in my academic work.

I would like to thank all members of the research group. They gave many helpful comments and suggestions on the experiment design, data processing and paper writing.

I want to express my deepest thanks to my family for their support, encouragement and love. I also appreciate my friends and the people who helped me for making my graduate program productive and enjoyable.

**Table of Contents**

**List of Tables**

**List of Figures**

# Chapter 1 Introduction

## 1.1 Research background

Plastics are increasingly demanded in industry, agriculture and daily life. They are commonly used in clothes, food packages and electronics, and most of them are for disposable use. Since the 1950s when plastics began to be used, plastic products grow exponentially and reached 368 million tons in 2019 (Ostle *et al.*, 2019; Akanyange *et al.*, 2021). The huge plastic production causes tons of plastic waste. The poor management and haphazard disposal of plastics make plastic waste enter and pollute the environment (Eriksen *et al.*, 2014; Akanyange *et al.*, 2021). About 60% of plastic products end up as plastic waste accumulated in landfill or environment (Geyer *et al.*, 2017). There is an estimation that 8 million tons of plastic waste are released into the ocean every year (Carbery *et al.*, 2018).

The average size of plastic wastes in the environment appears to be decreasing in the last several decades (Barnes *et al.*, 2009). Microplastics (MPs) defined as small plastics (< 5 mm in size) are of growing concern over the last few decades (Khatmullina and Isachenko, 2017). The amount of microplastic pollution grows and becomes ubiquitous (Yonkos *et al.*, 2014). MPs are one of the main pollutants in the environment because of their low degradability and easy transport, resulting the fact that they are found almost everywhere in the globe including the air, land, ocean, freshwater and even ice in the poles (Obbard *et al.*, 2014; Waldschläger and Schüttrumpf (2019); Padervand *et al.*, 2020). MPs in the environment are categorized into primary MPs and secondary MPs based on the sources. Primary MPs are the raw materials such as in cosmetics and personal care products, and secondary MPs are destructed from large plastics by physical, chemical and biological processes (Guo and Wang, 2019; Padervand *et*

*al.*, 2020). The primary MPs tend to be in regular shapes (e.g., spheres) and the shape of the secondary MPs tend to be various and random. The MPs detected in the environment mainly are pellets, fragments, disks, films and fibers (Hidalgo-Ruz *et al.*, 2012; Esiukova, 2017; Khatmullina and Isachenko, 2017).

The aquatic environment receives the majority of MP pollution (Zhao *et al.*, 2019). MPs threaten the aquatic environment and biota (Ma *et al.*, 2019). The pollutants in surrounding water are absorbed and concentrated by MPs (Guo and Wang, 2019). Moreover, MPs do harm to aquatic wildlife by directly ingestion as well as the toxicity of plastic constituents and absorbed contaminants, which also can be transferred in food chains and nets (Padervand *et al.*, 2020; Yu *et al.*, 2022).

There are an increasing number of research on MPs, but most of them focus on the abundance, occurrence and influence of MPs (Yu *et al.*, 2022). The dynamic property and physical transport of MPs are still poorly known, and one reason is that it is challenging to study the transport of MPs because of the wide ranges of MP size, shape and density (Khatmullina and Isachenko, 2017; Zhang, 2017). Given that about 50% of plastics are heavier than water and that in the marine environment more than 90% of MPs were found on the seafloor (Van Melkebeke *et al.*, 2020), the settling process is imperative for the studies on MP transport and fate.

The settling velocity $W$ is an important hydrodynamic parameter to assess the potential pathway and accumulated area of MPs with the interaction with currents, and therefore it is useful for the prediction of MP transport and fate in different aquatic conditions (Khatmullina and Chubarenko, 2019; Francalanci *et al.*, 2021). There are some previous studies on the settling velocity of non-MPs such as natural sediments and grains (e.g., Dietrich, 1982; Ferguson and

Church, 2004). Although the settling behaviors of MPs has similarity to sediments, to what extent and under what condition the results of sediments can be applied to MPs are still unclear due to the wider variety of MP shapes and different sizes and densities (Horton and Dixon, 2017; Waldschläger and Schüttrumpf, 2019). Especially for some 2-dimensional (e.g., disks) and 1-dimensional (e.g., fibers) MPs, the settling velocity formulas for sediments could be minor (Francalanci *et al.*, 2021).

The settling velocity of MP pellets, fragments and fibers has been studied to different extents (Bagaev *et al.*, 2017; Khatmullina and Isachenko, 2017; Kaiser *et al.*, 2019). It is demonstrated that MP density, shape and size exert impacts on the settling velocity. The settling velocity of some regular shaped MPs (e.g., spheres and short cylinders) exhibits reasonable consistency with those settling velocity formulas for non-MPs (Khatmullina and Isachenko, 2017). The settling velocity of some MPs including long cylinders, 2D fragments and irregular shaped particles, however, is much lower than those of the volume equivalent spheres and has a great deviation from the formulas developed for non-MPs (Kowalski *et al.*, 2016; Khatmullina and Isachenko, 2017; Kaiser *et al.*, 2019; Francalanci *et al.*, 2021). On the other hand, because of the great differences in shapes, the settling velocity formulas for MPs of other shapes (e.g., sphere) are also expected to be inappropriate for MP disks.

A few research concerned on the settling process of non-MP disks, and six types of trajectories of non-MP disks have been reported: steady falling, planar zigzag motion, transitional motion, spiral motion, chaotic motion, and tumbling motion (Field *et al.*, 1997; H. Zhong *et al.*, 2011). The results show that the size and density of non-MP disks impact the settling trajectory, and the trajectory changes from steady to unsteady with increasing Reynolds number (Stringham

*et al.*, 1969). These disk studies lay a foundation for the present study on MP disks.

So far, the terminal settling process in which MPs fall at their terminal settling velocity, has been the focus for the studies on MP settling (e.g., Khatmullina and Isachenko, 2017; Kaiser *et al.*, 2019; Francalanci *et al.*, 2021). However, the unsteady-state settling, including the acceleration process from the point of release till MPs reach the terminal velocity, has not been studied. The unsteady settling exists and could not be simply disregarded in certain situations such as settling in shallow water. The unsteady settling is also related to some other processes such as gravity particle separation and particle classification because assessing the paths of particles accelerating is important in these processes (Ferreira and Chhabra, 1998; Jalaal *et al.*, 2010). A few investigations on the acceleration process have been reported for non-MP spherical and non-spherical particles with rectilinear settling (Torabi and Yaghoobi, 2011; Jalaal *et al.*, 2012; Yaghoobi and Torabi, 2012; Yin *et al.*, 2017). The acceleration process of MP disks could differ significantly from that of spheres given the considerable deviation in the particle shape. Therefore, a thorough investigation on acceleration phase of MP disks is still essential for better understanding of MP transport and fate.

The literature above is in high level. A detailed literature review is provided in Chapter 2 and Chapter 3 of this thesis.

### 1.2 Knowledge gaps

Based on the literature review on the settling process of MPs, the following knowledge gaps are identified:

1) The settling of MP pellets, fragments, and fibers has been largely examined; however,

studies on MP disks (i.e., flat and thin MP particles) are scarce.

2) The research on MP settling has focused mainly on the mean terminal settling velocity; the settling trajectory and instantaneous settling velocity have not been investigated.

3) The acceleration settling process of particles (both plastic and non-plastic particles) has been barely investigated, not to mention those non-spherical particles with non-linear trajectory. No investigation has been conducted on the acceleration settling of MP disks.

### 1.3 Research goals and objectives

The overall objective is to fill the above-mentioned knowledge gaps. This research specifically aims to:

1) Understand the settling behaviors of MP disks including the settling trajectory, settling velocity (mean and instantaneous), and drag coefficient in both the acceleration and terminal settling processes.

2) Determine the effects of physical properties of MP disks (density, size and shape) on their settling processes.

3) Examine existing relations for MP disk settling, and proposed new relationships to better quantify or predict the settling.

The detailed objectives of Part I (Chapter 2) of this thesis are:

1) To investigate the settling trajectory and terminal velocity (both mean and instantaneous) in both vertical and horizontal directions for MP disk with different shapes (square, rectangle, and triangle), densities (1.038 - 1.343 g/cm$^3$) and sizes (1.5 - 5.0 mm).

2) To compare the settling behaviors of MP disks with non-MP disks and MPs of other shapes.

3) To determine the proper prediction for the settling trajectory, mean terminal settling velocity and drag coefficient of MP disks, including to propose new equations.

The detailed objectives of part II (Chapter 3) of the thesis are:

1) To study the settling behaviors including trajectory and velocity of MP disks with five release ways (different sides of MP disks facing downward), densities (1.038 - 1.343 $g/cm^3$), and release angles (0° - horizontal, 45° and 90° - vertical) in the acceleration phase.

2) To investigate the relationships between the settling motion (including the settling distance and maximum settling velocity) and physical characteristics of MP disks (including the density, shape and size), and to propose prediction equations.

3) To examine and discuss the drag coefficient (which changes with time) of accelerating MP disks with nonlinear trajectory.

**1.4 Thesis Outlines**

The thesis is written as paper-based format and organized into four chapters. In Chapter 1, general introduction and literature review on the topics of the thesis are presented, and knowledge gaps and objectives of this research are identified. Chapter 2 and Chapter 3 are the two parts (papers) of the main body. Chapter 2 (Part I) is "*Terminal Settling of Microplastic Disks in Stagnant Water*". Chapter 3 (Part II) is "*Acceleration Fall of Microplastic Disks in Stagnant Water*". Chapter 2 and Chapter 3 examine MP settling behaviors after and before reaching their terminal settling velocity, respectively. Chapter 2 is presented earlier because the current literature focuses on the terminal settling process, rather than the acceleration stage.

Chapter 4 provides general conclusions of this research and gives suggestions for future research.

## Chapter 2 Terminal Settling of Microplastic Disks in Stagnant Water

### 2.1 Introduction

Over the last several decades, the average size of plastic particles in the environment appears to be decreasing (Barnes *et al.*, 2009). Microplastics (MPs) are commonly defined as plastic particles of less than 5 mm (Alimi *et al.*, 2018). The abundant and worldwide distribution of MPs has grown (Barnes *et al.*, 2009; Yonkos *et al.*, 2014). MPs are widespread in the marine environment, lakes, rivers, and even in Arctic ice(Free *et al.*, 2014; Obbard *et al.*, 2014; Yang *et al.*, 2015). Typical shapes of collected microplastics are pellets, fragments, disks, films, and fibers (Esiukova, 2017; Khatmullina and Isachenko, 2017; Waldschläger and Schüttrumpf, 2019). MP pollution poses a threat to organisms and the environment (Ma *et al.*, 2019). MPs can be directly ingestion by aquatic biota because of their small size, resulting in digestive system obstructions and other negative physiological reactions (Yonkos *et al.*, 2014). Furthermore, the toxicity of plastic constituents and absorbed contaminants transferred along food chains and cause health issues (Padervand *et al.*, 2020; Yu *et al.*, 2022). In the environment, MPs have long-term durability and can be easily transported in the environment, which drives increasing concerns (Padervand *et al.*, 2020).

To understand and predict MP transport and fate in water, it is necessary to study the hydrodynamic properties of MPs including the settling process. The settling process is important as suggested by the fact that in the marine environment over 90% of MPs accumulate on the seafloor (Van Melkebeke *et al.*, 2020). Understanding the settling is also fundamental for the numerical modeling of MP transport and fate (Ballent *et al.*, 2013; Chubarenko *et al.*, 2016). In previous investigations, the settling velocities of MP pellets, fragments, and fibers

have been largely examined; however, studies on MP disks (i.e., flat and thin MP particles) are limited.

Kowalski *et al.* (2016) and Kaiser *et al.* (2019) revealed that settling velocities of MPs of irregular shapes were much lower than those of spheres of the same equivalent diameter. Khatmullina and Isachenko (2017) reported that previous formulas for terminal settling velocity of sediments were suitable for microplastics of MP spheres and short cylinders, but showed a great deviation for MP long cylinders. Waldschläger and Schüttrumpf (2019) proposed formulas for the settling and rising velocities of regular and irregular MPs with diverse densities and sizes. Van Melkebeke *et al.* (2020) were the first who examined MP film settling velocity in ethanol and regarded sphericity as a good shape descriptor for the films. Francalanci *et al.* (2021) showed the difference between the settling velocity of 2D MP fragments and MP spheres and developed a universal model for the prediction of the settling velocity of 3D (e.g., pellets), 2D (e.g., disks), and 1D particles (e.g., fibers). The influence of particle shapes on the settling velocity is attributed to the effects of shapes on the particle Reynolds number ($Re$) and the drag coefficient ($C_D$) during the settling process (Khatmullina and Isachenko, 2017; Yu *et al.*, 2022). The settling velocity formulas for MPs of other shapes are expected to be not appropriate for MP disks due to the great differences in shapes. Additionally, so far, studies on MP settling have focused on the mean terminal settling velocity; the settling trajectory and instantaneous velocity of MPs have not been reported. Therefore, it is imperative to further investigate these aspects, particularly for MP disks.

Up to now, there have been a few studies on non-MP disks including large (5 - 60 mm) disks of plastic, lead, titanium, steel, and aluminum (Willmarth *et al.*, 1964; Stringham *et al.*, 1969;

Zhong *et al.*, 2011; Song *et al.*, 2017). The settling trajectories of these disks were different depending on their sizes and densities. Several dimensionless parameters have been used to characterize the settling behavior of disks: the particle Reynolds number of disks $Re_d = Wd/v$, the dimensionless moment of inertia $I^* = \pi h\rho_s/(64d\rho)$, and the Archimedes number $Ar = \sqrt{3gh(\rho_s - \rho)/16\rho}d/v$, where $W$ is the mean settling velocity, $d$ and $h$ are the diameter and thickness of disks, $\rho_s$ is the density of disks, and $\rho$ and $v$ are the density and kinematic viscosity of the ambient fluid, $g$ is the gravitational acceleration (Willmarth *et al.*, 1964; Field *et al.*, 1997; Zhong *et al.*, 2011; Auguste *et al.*, 2013). With the increase of $Re$, the non-MP disk settled from steadily to unsteadily, which was related to the instability of pressure forces in the wake (Stringham *et al.*, 1969). The dimensionless moment of inertia $I^*$ was also correlated with particle stability, and a $Re_d$ - $I^*$ phase diagram was proposed based on metal and plastic disks (Willmarth *et al.*, 1964; Stringham *et al.*, 1969). Field *et al.* (1997) named four settling trajectories of metal disks - steady falling, periodic-oscillating motion, chaotic motion, and tumbling motion - and they proposed the boundaries of the four regimes (steady, periodic, chaotic and tumbling regimes) using the $Re_d$ - $I^*$ diagram. Zhong *et al.* (2011) further reported three unsteady settling trajectories: planar zigzag, transitional and spiral, and extended the $Re_d$ - $I^*$ phase diagram by replacing the periodic regime with the planar zigzag, transitional and spiral regimes. Auguste *et al.* (2013); Wang *et al.* (2016) investigated the impact of the aspect ratio of circular disks on the settling behaviors by numerical simulations.

Although existing studies have discussed the distinct settling behaviors of non-MP disks, no studies on MP disks have been reported regarding settling trajectories and velocities. Moreover, non-MP disks studied in the literature are mainly circular disks with sizes larger than 5 mm,

and the settling behaviors of disks of other shapes have received limited investigation. Given the difference between MP and non-MP disks in sizes, densities, and shapes, MP disks likely have different settling behaviors. Hence, to further understand the settling process of various-shaped MPs that exist in the environment, a detailed study is imperative.

To fill the above-mentioned knowledge gaps, we conducted settling experiments on the settling trajectory and terminal velocity (both mean and instantaneous) of MP disks in the water. A total of four types of MPs were used with different shapes (square, rectangle, and triangle), densities (1.038 - 1.343 g/cm$^3$), and sizes (1.5 - 5.0 mm). The settling trajectory and velocity were analyzed in both vertical and horizontal directions to further understand the settling behavior of MP disks. The drag coefficient was also examined. Finally, a new equation was developed for predicting the terminal settling velocity of MP disks, and the $Re_d$ - $I^*$ phase diagram was extended for MP disks.

### 2.2 Theoretical foundation

Settling velocity formulas from previous studies were mainly developed for sediments (e.g., (Dietrich, 1982; Ferguson and Church, 2004; Z. Song *et al.*, 2008). For non-MP smooth spheres, Dietrich (1982) correlated the dimensionless diameter $D^*$ with the dimensionless velocity $W^*$:

$$\begin{aligned}\log(W^*) = &-3.76715 + 1.92944\log(D^*) - 0.09815\log(D^*)^2 \\ &-0.00575\log(D^*)^3 + 0.00056\log(D^*)^4\end{aligned} \tag{2.1}$$

where $D^* = \frac{(\rho_s - \rho)gD_n^3}{\rho\nu^2}$, $D_n$ is the nominal diameter of particles, which is the diameter of a sphere having the same volume as the particle, i.e., $D_n = \sqrt[3]{\frac{6V}{\pi}}$; and $W^* = \frac{\rho W^3}{(\rho_s - \rho)g\nu^2}$, in which $W$ is the terminal settling velocity.

To describe the impacts of particle size, density shape, and roundness on the terminal settling velocity, Dietrich (1982) proposed the formula for sediments with the Corey shape factor *CSF* and Powers roundness coefficient *P*:

$$
\begin{aligned}
W^* &= R_3 10^{R_1+R_2} \\
R_1 &= \log(W^*) = -3.76715 + 1.92944\log(D^*) - 0.09815\log(D^*)^2 \\
&\quad -0.00575\log(D^*)^3 + 0.00056\log(D^*)^4 \\
R_2 &= \log\left(1-\frac{1-CSF}{0.85}\right) - (1-CSF)^{2.3}\tanh[\log(D^*)-4.6] \\
&\quad +0.3(0.5-CSF)(1-CSF)^2[\log(D^*)-4.6] \\
R_3 &= \left[0.65-\left(\frac{CSF}{2.83}\tanh(\log(D^*)-4.6)\right)\right]^{1+\frac{3.5-P}{2.5}}
\end{aligned}
\tag{2.2}
$$

where *CSF* is a commonly-used shape descriptor defined as $c/(ab)^{1/2}$, where *a*, *b* and *c* are the longest, intermediate, and shortest lengths of the particle in three perpendicular axes, respectively. *CSF* varies from nearly 0 (thin disk) to 1 (perfect sphere) (Corey, 1949; Francalanci *et al.*, 2021). *P* is defined by six roundness classes from very angular ($P = 1$) to well-rounded ($P = 6$) particles.

Ferguson and Church (2004) proposed a settling velocity equation in the entire range of viscous to turbulent regimes for all grains sizes:

$$
W^* = \frac{D^{*2}}{(C_1 + \sqrt{C_2 0.75 D^{*2}})^3} \tag{2.3}
$$

For smooth spheres, $C_1 = 18$, $C_2 = 0.4$; for natural grains, $C_1 = 18$, $C_2 = 1.0$; for very angular grains, $C_1 = 24$, $C_2 = 1.2$. Eqn. (2.3) gave a good fit to data of non-MP grains, such as quartz and river sands.

Camenen (2007) presented a $W^*$formula for particles of all kinds of material and any shapes.

$$
\begin{aligned}
W^* &= \frac{1}{D^*}\left[\sqrt{\frac{1}{4}\left(\frac{A}{B}\right)^{\frac{2}{m}} + \left(\frac{4}{3}\frac{D^*}{B}\right)^{\frac{1}{m}}} - \frac{1}{2}\left(\frac{A}{B}\right)^{\frac{1}{m}}\right]^{3m} \\
A &= a_1 + a_2\left[1 - \sin\left(\frac{\pi}{2}CSF\right)\right]^{a_3} \\
B &= b_1 + b_2\left[1 - \sin\left(\frac{\pi}{2}CSF\right)\right]^{b_3} \\
m &= m_1 \sin^{m_2}\left(\frac{\pi}{2}CSF\right)
\end{aligned}
\tag{2.4}
$$

where $a_1 = 24$, $a_2 = 100$, $a_3 = 2.1 + 0.06P$, $b_1 = 0.39 + 0.226(6 - P)$, $b_2 = 20$, $b_3 = 1.75 + 0.35P$, $m_1 = 1.2 + 0.12P$, and $m_2 = 0.47$. The three coefficients of $A$, $B$ and $m$ in the formula had explicit relationships with particle $CSF$ and roundness $P$. This equation showed a decent performance with experimental data of non-MPs such as plastic cylinders and sands.

Song *et al.* (2008) developed a quasi-theoretical equation of $W^*$ for natural sediments:

$$
W^* = D^{*2}\left[\left(\frac{3A}{4}\right)^{\frac{2}{n}} + \left(\frac{3B}{4}D^*\right)^{\frac{1}{n}}\right]^{-\frac{3n}{2}} \tag{2.5}
$$

where $A = 32.2$, $B = 1.17$ and $n = 1.75$ are constants.

The drag coefficient ($C_D$) is an essential parameter for particle transport in fluids. Particle density, size, and shape exert an important impact on $C_D$ (Haider and Levenspiel, 1989; Hölzer and Sommerfeld, 2008). When a particle reaches terminal settling velocity, the drag force equals the gravitational force.

$$
\frac{1}{2}C_D\rho A W^2 = (\rho_S - \rho)gV \tag{2.6}
$$

where $A$ is the projected area of the particle, and $V$ is the volume of the particle.

There were numerous investigations about $C_D$ of particles of different shapes. Clift and Gauvin

(1971) derived $C_D$ for smooth spheres with $Re < 3 \times 10^5$:

$$C_D = \frac{24}{Re}(1 + 0.15Re^{0.687}) + \frac{24}{1 + \frac{42500}{Re^{1.16}}} \tag{2.7}$$

Haider and Levenspiel (1989) introduced the sphericity $\Phi$ in their $C_D$ formula for non-MP particles (metals and plastics) of regular shapes including spheres, cubes, and disks:

$$\begin{aligned} C_D &= \frac{24}{Re}(1 + ARe^B) + \frac{C}{1 + \frac{D}{Re}} \\ A &= \exp(2.3288 - 6.4581\Phi + 2.4486\Phi^2) \\ B &= 0.0964 + 0.5565\Phi \\ C &= \exp(4.905 - 13.8944\Phi + 18.4222\Phi^2 - 10.2599\Phi^3) \\ D &= \exp(1.4681 + 12.2584\Phi - 20.7322\Phi^2 + 15.8855\Phi^3) \end{aligned} \tag{2.8}$$

where $\Phi$ is defined as $A_{sph}/A_{act}$, in which $A_{sph}$ is the surface area of a sphere with the same volume as the particle and $A_{act}$ is the actual surface area of the particle. This equation is valid for $Re < 2.6 \times 10^5$.

Cheng (2009) proposed a more accessible and easier equation for spheres with better representation for $Re < 2 \times 10^5$

$$C_D = \frac{24}{Re}(1 + 0.27Re)^{0.43} + 0.47[1 - exp(-0.04Re^{0.38})] \tag{2.9}$$

Hölzer and Sommerfeld (2008) divided sphericity $\Phi$ into two parts - crosswise sphericity ($\Phi_\perp$) and lengthwise sphericity ($\Phi_\parallel$) based on the falling orientation of non-spherical particles. $\Phi_\perp$ is the ratio of $A_{sph}$ to the projected cross-section area of the particle perpendicular to the flow, and $\Phi_\parallel$ is the ratio of $A_{sph}$ to the difference between half of $A_{act}$ and the mean longitudinal projected cross-section area of the particle. They proposed an equation of $C_D$ for particles of various shapes over the entire range $Re$:

$$C_D = \frac{8}{Re}\frac{1}{\sqrt{\Phi_{//}}} + \frac{16}{Re}\frac{1}{\sqrt{\Phi}} + \frac{3}{\sqrt{Re}}\frac{1}{\Phi^{\frac{3}{4}}} + 0.421^{0.4(-\log\Phi)^{0.2}}\frac{1}{\Phi_{\perp}} \quad (2.10)$$

Dioguardi *et al.* (2018) developed a new equation using a shape factor $\Psi$ ($\Psi = \Phi/\chi$) that included both sphericity $\Phi$ and circularity $\chi$ of a particle:

$$C_D = \frac{24}{Re}\left(\frac{1-\Psi}{Re}+1\right)^{0.25} + \frac{24}{Re}\left(0.1806\,\mathrm{Re}^{0.6459}\right)\Psi^{-Re^{0.08}} + \frac{0.4251}{1+\frac{6880.95}{Re}\Psi^{5.05}} \quad (2.11)$$

where $\chi$ is the ratio of the maximum projected perimeter of the particle to the perimeter of the circle equivalent to the maximum projected area of the particle. This equation is valid for irregular particles with $3 \times 10^{-2} < Re < 1 \times 10^4$. Waldschläger and Schüttrumpf (2019) developed an equation for MP sphere and fragments with $0.1 < Re < 1 \times 10^4$, and used the Corey shape factor (*CSF*) as a parameter.

$$C_D = \frac{3}{CSF\ \sqrt[3]{Re}} \quad (2.12)$$

## 2.3 Materials and methods

### 2.3.1 MP particles

Four types of MP materials were used in the experiment: polyvinyl chloride (PVC, $\rho_s$ = 1.343 g/cm$^3$), polyethylene terephthalate (PET, $\rho_s$ = 1.319 g/cm$^3$), polycarbonate (PC, $\rho_s$ = 1.161 g/cm$^3$), and acrylonitrile butadiene styrene (ABS, $\rho_s$ = 1.038 g/cm$^3$). They are commonly used plastics in daily life, e.g., PVC for pipes and guttering, PET for drinks bottles and packaging, PC for lenses, and ABS for electronic equipment cases (Ghosh *et al.*, 2013; W. C. Li *et al.*, 2016; Andrady, 2017). The MP disks were cut from large plastic sheets ordered online.

The MP disks used in this study had side lengths $l$ = 1.5 mm - 5.0 mm and thicknesses $h$ = 0.15

mm - 0.50 mm (Table 2.1), for which the measurement was conducted with a digital caliper (accuracy level of ± 0.001 mm). The aspect ratios *h/l* were around 0.1 and *CSF* was from 0.06 - 0.14, which were within the *h/l* and *CSF* ranges of 0.001 - 0.200 used in the previous studies of circular disks (Willmarth *et al.*, 1964; Stringham *et al.*, 1969; H. Zhong *et al.*, 2013; Song *et al.*, 2017; Mrokowska, 2020). Three shapes of MP disks were used in this study, including square, rectangle, and triangle (Figure 2.1). Rectangular and triangular disks were obtained by cutting square disks in half.

The MP disk density was determined based on the titration method (ISO 1183-1, 2012) and further confirmed with the density values obtained from the online MP sellers. The density test was conducted in a glass beaker with 100 ml of distilled water. Ten particles were randomly selected from each polymer type and put in the glass beaker. After all the particles had fallen to the bottom, zinc chloride solution ($\rho$ = 1.600 g/cm$^3$) was added slowly by a burette. After each addition, the solution was stirred and mixed. With more zinc chloride solution added, particles started rising and stayed suspended for at least 1 min. The solution density equaled the density of particles at this time. 1 ml solution was delivered to a beaker by an automatic pipette and weighed on an analytical balance (± 0.001 g accuracy) to calculate the density.

To compare the measured terminal settling velocity between different shapes and materials in this study and previous studies, the velocity and particle size were presented in the form of $W^*$ and $D^*$. The drag coefficient $C_D$ was obtained with Eqn. (2.6) and the particle Reynolds number was calculated as Eqn. (2.13):

$$Re = \frac{WD_n}{\nu} \tag{2.13}$$

As the MP disks in this study are thin (i.e., $h << l$), there would be a deviation using $D_n$ to

describe the size of the MP disks where the MP disk is regarded as a sphere. In the studies of non-MP disks, the characteristic lengths of circular disks are often expressed by the diameter of the circular surface instead of $D_n$ (Field *et al.*, 1997; Zhong *et al.*, 2011). Thus, to reduce the error of treating the disk as a sphere and compare it with non-MP circular disks, we used the maximum diameter $D_m$ to calculate $Re$ (named disk Reynolds number $Re_d$, where the subscript stands for disk) and the dimensionless moment of inertia $I^*$ in MP disk settling behavior analysis, as shown in Eqn. (2.14) and Eqn. (2.15). Herein, $D_m$ is the diameter of a circle having the same area as the maximum projected area of the particle: $D_m = \sqrt{\frac{4A}{\pi}}$.

$$Re_d = \frac{WD_m}{\nu} \tag{2.14}$$

$$I^* = \frac{\pi h \rho_s}{64 \rho D_m} \tag{2.15}$$

2.3.2 Experiment setup and procedure

The settling experiment was conducted in a plexiglass column with a square cross-section of 20 × 20 cm and a height of 120 cm (Figure 2.1). The cross-sectional dimensions of the column were much larger than the disks, and therefore, wall effects were ignored. The column was filled with tap water at room temperature of 20 ± 0.5 °C. To trace the settling trajectory of a single disk, a dot was marked on the centroid of the disk surface on each side. All disks were placed in a 50 ml glass beaker filled with water for 3 hours to avoid the static surface charge and expelled air bubbles on the surface before the settling experiment. The disk was delivered from the beaker to the center of the column by a tweezer. The disk was immersed and released at 2 cm below the water surface to avoid surface tension, and then it settled freely. A high-speed camera (Phantom v211, USA) was used to record the settling process of the disk at a frame rate

of 100 fps and a resolution of 1280 × 720 pixels. The entire settling process of each MP disk was recorded from the water surface to the column bottom, and the settling velocity was found to not increase after 15 cm below the surface. As this study focused on the terminal velocity and trajectory, the videos taken from 15 cm to 105 cm were analyzed to avoid the initial acceleration phase and the final deceleration near the column bottom. After one MP disk reached the bottom, the next disk would not be released until the water was still.

The settling trajectory of each MP disk was analyzed with the software *ImageJ* (National Institutes of Health, USA). The terminal settling trajectory was obtained by connecting the dots marked on the disk in each image. The *x*-direction was defined as the vertically downward direction, while the *y*-direction was the horizontal direction (Figure 2.1). The terminal settling velocity ($W$) was the mean of the terminal vertical velocity of the disk calculated every 30 cm. The instantaneous terminal settling velocities in the $x$ and $y$ directions, $W_x$ and $W_y$, were obtained from processing every two images (i.e., every 0.02 s) after disks reached the terminal velocity. The relative error *Err* was used in this study.

$$Err = \frac{1}{N}\sum \frac{W_{cal} - W_{mea}}{W_{mea}} \times 100\% \tag{2.16}$$

where $W_{mea}$ is the measured settling velocity, $W_{cal}$ is the calculated settling velocity, and $N$ is the number of measurements.

Prior to the MP experiments, glass spheres were used to validate the measurement method of settling velocity in this study. The glass spheres had a density of 2.460 g/cm$^3$ and diameters of 5.0 ± 0.1 mm, 3.0 ± 0.05 mm, 2.7 ± 0.1 mm, and 0.7 ± 0.05 mm. The measured settling velocities of glass spheres were compared with the theoretical settling velocity equation for

spheres developed by Dietrich (1982) (Eqn. 2.1). Figure 2.2 shows that the measured settling velocities fitted Eqn. (2.1) well with the relative error of $Err$ = 0.02% and the coefficient of determination $R^2$ = 0.997. This suggests that the experimental setup and methodology are valid for measuring the terminal settling velocity of particles.

## 2.4 Results and discussion

### 2.4.1 Settling trajectory

Three types of settling trajectories of MP disks were observed in the experiments: steady, zigzag and combination of zigzag and transitional (Table 2.2). The trajectory name is adapted from Zhong *et al.* (2011). The MP disks with the side length $l$ < 5mm and ABS disks with $l$ = 5mm have a steady vertical falling (see ABS trajectory in Figure 2.1c). The PC, PET, and PVC disks with $l$ = 5 mm showed an unsteady falling, which have secondary motions during the settling process: oscillations and rotations and fall in a zigzag path (see their trajectories in Fig. 1c). For the disks with unsteady falling, the secondary motions vary with the shape of MP disks. For example, PC, PET, and PVC square disks oscillate (e.g., move from left to right and back to left) during the falling and have a zigzag trajectory. PC, PET, and PVC rectangular and triangular disks also oscillate during the falling. But the direction of oscillation is not fixed all the time, it rotates and disks spin around their vertical revolution axis occasionally. We found the similarity of this kind of settling trajectory with two trajectories reported by Zhong *et al.* (2011) - zigzag and transitional. The trajectory of rectangular and triangular disks tends to be a combination of zigzag and transitional trajectories. The possible reason of the difference in trajectory is that the shape affects the ambient fluid flow, which affects shear drag and pressure drag and then impacts the settling behaviors of particles (Stringham *et al.*, 1969).

In each type of plastic, the settling trajectory is different with the MP size and shape. Specifically, the PVC, PET and PC disks with $l$ = 5 mm have the unsteady settling trajectory; while those with $l$ = 3 mm and $l$ = 1.5 mm the steady settling trajectory. Besides, the PVC, PET and PC square disks with $l$ = 5 mm with zigzag settling trajectory are different from those rectangular and triangular disks that have the combination of zigzag and transitional trajectory. For MP disks of the same size and shape, the MP material is also important for the trajectory. for example, the settling trajectory of ABS disks with $l$ = 5 mm is rectilinear; it is different from that of other materials that have non-linear trajectory as stated above. Overall, the density, size, and shape of MP disks affect settling trajectories. The settling trajectory of disks is related to several hydrodynamic parameters such as Reynolds number ($Re_d$) and Archimedes number ($Ar$). A few studies discussed the settling trajectories of non-MP disks with various dimensionless parameters, such as the $Re_d$ - $I^*$ diagram of Field *et al.* (1997), the $Ar$ - $I^*$ diagram of Auguste *et al.* (2013), and the $\rho_s/\rho$ - $l/h$ diagram of Wang *et al.* (2016). The $Ar$ - $I^*$ diagram is for thin disks with the $Ar$ range of 0 to 55, which does not apply well to our data because our $Ar$ value ranges from 15 to 100. The $\rho_s/\rho$ - $l/h$ diagram is not comprehensive for the settling trajectory prediction because it does not include the impact of disk size on the trajectory, while our experiment results show such impact is important for the MP disks. The $Re_d$ - $I^*$ phase diagram has a wide range of $10 < Re_d < 10^5$ and takes into account the impact of disk size, thickness and $\rho_s/\rho$. Zhong *et al.* (2011) have extended the $Re_d$ - $I^*$ diagram, but the region of $10^2 < Re_d < 10^3$ and $10^{-3} < I^* < 10^{-2}$ in the periodic regime is still blank (Figure 2.3). Since the $Re_d$ - $I^*$ diagram focuses on non-MP disks, we extended the $Re_d$ - $I^*$ diagram of Field *et al.* (1997); Zhong *et al.* (2011) to study the settling trajectory of MP disks (Figure 2.3).

Figure 2.3 shows our results are around $2 \times 10^1 < Re_d < 2 \times 10^2$ and $I^* = 6 \times 10^{-2}$. Green square data points represent the MP disks having zigzag trajectories. Blue triangle data points represent the MP disks where both zigzag and transitional trajectories were observed during their settling. Since they had a combination trajectory of zigzag and transitional, the boundary between the zigzag motion area and the transitional motion is expected to pass through the blue data points. Red circle dots represent the MP disks with steady vertical settling but they show some deviations from the existing, non-MP, steady regime boundary. The red dots with $Re_d > 10^2$ fall in the periodic regime but have a steady settling. This is possibly due to the different physical characteristics among the studied disks such as material and size. The boundary of the steady regime with $4.5 \times 10^{-3} < I^* < 5.5 \times 10^{-3}$ was determined based on the data of circular steel and lead disks with diameter $d$ = 5.1 - 18.0 mm from Field *et al.* (1997). The deviated red dots in this study are for square PVC, PET and PC disks with length $l$ = 3 mm and square ABS disks with length $l$ = 5 mm. Stringham *et al.* (1969) indicated shape, sharp corners and surface roughness of particles impacts their settling behaviors by changing the shear and pressure drag. Hence, the deviation is possibly due to the distinction of roundness (circular vs square), surface roughness (metals vs plastics) and size (5.1 - 18 mm vs. 3 mm) of the disks between Field *et al.* (1997) and this study. In brief, Figure 2.3 can be used to predict the settling trajectory types of MP and non-MP disks. Meanwhile, it is important to point out that more experiments are needed to further validate and expand Figure 2.3 for MPs.

### 2.4.2 Instantaneous terminal settling velocity

The instantaneous settling velocity of MP disks with $l$ = 3 mm and 1.5 mm is constant and equals the mean settling velocity. The instantaneous settling velocity of MP disk with $l$ = 5 mm

is more complicated. It oscillates with time and is inconsistent with the mean settling velocity. Thus, we focus on the settling velocity of the MP disk with $l$ = 5 mm. Figure 2.4 presents the instantaneous terminal settling velocity of each shaped MP disk with $l$ = 5 mm. The ABS disks fall steadily and therefore $W_x$ and $W_y$ are constants ($W_{x,\ square}$ = 38.5 mm/s, $W_{x,\ rectangle}$ = 39.2 mm/s, $W_{x,\ triangle}$ = 35.6 mm/s; and $W_y$ = 0 for all the three shapes). The PVC, PET and PC disks follow zigzag paths (Figure 2.1c) and their instantaneous settling velocities fluctuate periodically with time with different amplitudes (Figure 2.4). The values of $W_x$ are positive since disks settle along the vertical ($x$) direction, while $W_y$ has positive and negative values since the trajectory is symmetric about the $x$-axis. The minus values of $W_y$ represent the velocities in opposite direction along the $y$-axis. The oscillation frequency, amplitude, maximum and minimum values of the instantaneous settling velocity are summarized in Table 2.3. In general, the oscillation frequency of $W_x$ (2.91 - 4.57 Hz) is twice of the frequency of $W_y$ (1.46 - 2.27 Hz) resulting from the symmetry of the settling trajectory. The amplitude of $W_y$ (23.2 ± 8.0 mm/s) is about twice the amplitude of $W_x$ (10.0 ± 2.5 mm/s). These relationships do not exhibit obvious trends with different sizes and densities of MP disks. Zhong *et al.* (2013) who tested Plexiglas disks with diameters > 20 mm at $Re_d$ = 1650 (6 – 12 times of $Re_d$ in this study), also found the frequency of $W_x$ is twice the frequency of $W_y$.

Both the density and shape of MP disks exert an impact on the instantaneous settling velocity. For the same shaped MP disk, frequency, extreme (maximum and minimum) values and amplitude of instantaneous velocity always decrease with the decrease of density from 1.343 (PVC) to 1.161 g/cm$^3$ (PC) (Table 2.3). The density of PET (1.319 g/cm$^3$) is close to that of PVC, and thus the decrease of these velocity values is small from PVC to PET disks. For

rectangular and triangular disks, PVC disks have the largest $W_{x,max}$ (maximum vertical settling velocity), $W_{x,min}$ (minimum vertical settling velocity) and $W_{y,max}$ (maximum horizontal settling velocity) among the three materials (PVC, PC and PET), while PC disks have the smallest. For square disks, the PVC disk also have the largest $W_{x,max}$ (62.3 mm/s), $W_{x,min}$ (35.3 mm/s) and $W_{y,max}$ (35.2 mm/s) and PC disks have the smallest $W_{x,max}$ (46.9 mm/s) and $W_{y,max}$ (15.4 mm/s). PET disks, however, have the smallest $W_{x,min}$ (28.7 mm/s), although their density (1.319 g/cm$^3$) is much larger than that of PC (1.161 g/cm$^3$). The amplitude for $W_x$ of rectangular disks has a slight decreasing trend from 9.9 mm/s to 7.3 mm/s with decreasing MP density from PVC to PC; but it shows different trends for square and triangular disks - PET disks have the largest values (15.0 mm/s for square; 10.0 mm/s for triangular), followed by PVC disk (7.9 mm/s for square; 9.3 mm/s for triangular) and then PC disk (15.0 mm/s for square; 10.0 mm/s for triangular). The results of amplitude for $W_y$ are consistent with that for $W_x$. The shapes of MP disks also affect the extreme values and amplitude of instantaneous settling velocity. For the same material, square disks have around 10% larger maximum velocity as well as around 40% larger amplitude of $W_x$ and $W_y$ than rectangular and triangular disks (except PC triangular disks). Unlike the density of disks, shapes do not impact the frequency. The frequency of $W_x$ is around 4.56 Hz for PVC disks, 4.40 Hz for PET disks and 3.10 Hz for PC disks of all three shapes (square, rectangle and triangle).

Figure 2.5 demonstrates the relationship between MP disk position and the instantaneous settling velocities, where the origin (x, y) = (0, 0) is the position of an MP disk (the marked dot on the disk) at $t = 0$. $t = 0$ is the time when the disk face is perpendicular to the flow. The values of ABS disks are a single point in each sub-figure because they fall steadily without fluctuation

in $W_x$ and $W_y$, while the data points of each of the other three MP disks (PVC, PET, and PC) distribute like an open ellipse since $W_x$ and $W_y$ oscillate periodically with time. In the vertical direction (left column of Figure 2.5), the ordinates of ABS and the elliptic centers of the other three materials represent the mean terminal settling velocity $W$. For instance, in Figure 2.5(a) left, the ordinates of green dots and the elliptic centers are: 24.0 mm/s for ABS, 38.5 mm/s for PC, 43.0 mm/s for PET, and 46.5 mm/s for PVC, which are their terminal velocities. The lengths of the semi-major axis of the ellipses represent the amplitudes of $W_x$. The black dots (PVC) have the longest semi-major axis while blue dots (PC) have the shortest semi-major axis, which appears to be related to MP density.

In the horizontal $y$ direction (right column of Figure 2.5), all the centers of the ellipses are (0 mm, 0 mm/s), and the semi-major axis and semi-minor axis represent the amplitudes of the trajectory and $W_y$, respectively. MP disk with a smaller density has smaller major and minor axes of the ellipse: the major/minor axis of the blue dots (PC, 1.161 g/cm$^3$) is smaller than that of red (PET, 1.319 g/cm$^3$) and black (PVC, 1.343 g/cm$^3$) dots. The amplitude of $W_y$ has been discussed earlier and thus we focus on the amplitude of the trajectory (semi-major axis) here. The semi-major axis appears to be related to both the MP disk density and shape. PVC disks have the largest semi-major axis (1.9 mm for square disks, 1.5mm for rectangular disks and 1.5mm for triangular disks), followed by PET disks (1.8 mm for square disks, 1.4mm for rectangular disks and 1.5mm for triangular disks) and PC disks (1.4 mm for square disks, 0.8 mm for rectangular disks and 1.4 mm for triangular disks). The difference between the amplitude of PVC and PET disks is small, which is due to the similarity in density of these two types of MP disks. MP disks with $l$ = 5 mm but of different shapes also vary in the length of

the semi-major axis. For PVC and PET disks, the square disks have the largest semi-major axis (2.1 mm for PVC; 1.8 mm for PET), and the rectangular and triangular disks have a small difference (within 12%). The amplitude of translational motion is related to $I^*$ (Willmarth *et al.*, 1964). The square disk with larger $I^*$ has a larger amplitude. Rectangular and triangular disks with the same $I^*$ has almost the same amplitude. But for PC disks, square and triangular disks have the same semi-major axis (1.4 mm) and they are 55% larger than that of rectangular disks.

2.4.3 Mean terminal settling velocity and drag coefficient

The measured mean terminal settling velocities, $W$, for around 300 MP particles are summarized in Table 2.2 The settling velocity ranges from 19.63 mm/s of the lightest and smallest ABS disks to 48.84 mm/s of the heaviest and largest PVC disks. In each MP material set, $W$ increases with increasing length $l$ and varies with the shape of disks. In addition, the influence of shape is also related to the settling motion. For MP disks with the steady settling trajectory (e.g., ABS disks with $l$ = 5 mm as well as PVC, PET and PC disks with $l$ = 3 mm), $W$ is positively linear correlated with the nominal diameter $D_n$ ($R^2$ = 0.953 ± 0.03). For MP disks of the same material, square MP disks that have the largest $D_n$ compared to other shapes with the same length $l$ ($D_{n,square} = 1.26D_{n,rectangle} = 1.26D_{n,triangle}$) have the greatest $W$ ($W_{square}$ = 1.14 -1.18 $W_{rectangle}$ = 1.14 -1.18 $W_{triangle}$). Rectangular and triangular disks with the same $D_n$ almost have the same $W$, and the difference is < 3%. For disks with unsteady settling trajectory (e.g., PVC, PET and PC disks of $l$ = 5 mm), $W$ does not show a positive linear correlation with $D_n$ with $R^2 < 0.1$. For the MP disks with the same $l$, $W$ exhibits a slight change with the shape of MP disks ($W_{square}$ = 0.97 - 0.98 $W_{rectangular}$ = 1.06 - 1.10$W_{triangular}$). Square disks do not have

the largest $W$ despite having the highest $D_n$, and rectangular and triangular disks with the same $D_n$ have clearly different $W$. In short, our results suggest that for MP disks with steady settling, $D_n$ has an essential influence on the mean terminal velocity $W$ and the influence of disk shape can be ignored; but for MP disks with unsteady settling, shapes exerted a clear impact on $W$ and the impacts of $D_n$ is not obvious.

Figure 2.6 shows that with the increase of MP disk density and the nominal diameter $D_n$, the terminal settling velocity $W$ increases. The data points with $D_n > 2$ mm represent the MP disks with side length $l = 5$ mm, the data points with 1.3 mm $< D_n <$ 1.8 mm represent disks with $l =$ 3 mm, and the data points with $D_n < 1.3$ mm represent disks with $l = 1.5$ mm. The $W$ - $D_n$ relationship is non-linear and similar for each material. The terminal settling velocity $W$ increases less rapidly with the increase of $D_n$ as seen from the decrease of the slope of the $W$ - $D_n$ relationship.

Figure 2.7 exhibits the relationship between the dimensionless terminal settling velocity $W^*$ and the dimensionless particle diameter $D^*$ for MP particles of different shapes. It is shown that at the same $D^*$, the MP particles with greater *CSF* have a higher $W^*$. The data points of MP pellets (black triangles in Figure 2.7) collected from the literature (Hazzab *et al.*, 2008; Kowalski *et al.*, 2016; Khatmullina and Isachenko, 2017; Francalanci *et al.*, 2021) have the largest *CSF* (0.8 - 1.0), which are on top of other data. The $W^*$ data points of MP cylinders (blue stars in Figure 2.7) with *CSF* values of 0.6 - 1.0 from Khatmullina and Isachenko (2017) are slightly lower. The data points of irregular MP fragments (green crosses in Figure 2.7) with *CSF* values of 0.1 - 0.6 from Kowalski *et al.* (2016) are scattered, probably due to their irregular shapes and generally have further lower $W^*$. The data points of 2D MP fragments with irregular

shapes of top surface (red empty circles in Figure 2.7) from Francalanci *et al.* (2021) have *CSF* = 0.02 to 0.12, which are within the *CSF* range of a disk, and thus they can be regarded as disk-like MPs. The orange diamonds represent thin MP films settling in ethanol from Van Melkebeke *et al.* (2020). The MP films with even smaller *CSF* (< 0.061) has lower $W^*$ than MP disks. The present data points (red filled circles in Figure 2.7) and those of Francalanci *et al.* (2021) suggest that $W^*$ values of MP disks and 2D (disk-like) fragments are lower than those of MP pellets, cylinders and some of the irregular MP fragments, but higher than MP films.

Figure 2.8 compares MP and non-MP disk experimental data collected from this study and the literature with the existing $W^*$ - $D^*$ formulas for spheres, sediments and non-MP disks. Khatmullina and Isachenko, (2017) and Francalanci *et al.* (2021) show the non-MP sphere formulas of Dietrich (1982) and Ferguson and Church (2004) (with $C_1$ = 18, $C_2$ = 0.4) gave a reasonable prediction for MP spheres with $D_n$ of 0.9 - 5.0 mm. However, the $W^*$ data points of MP disks are considerably lower than the formulas for spheres and sediments from Dietrich (1982), Ferguson and Church (2004), Camenen (2007) and Song *et al.* (2008), which can be explained as follows: Compared with spheres, disks of the same $D_n$ have a larger surface area, resulting in higher pressure and friction drag and thus a greater resistance to motion and therefore a lower *W*. (Dietrich, 1982; Kowalski *et al.*, 2016). Moreover, disks are flattened which induces flow separation and leads to larger drag coefficient and smaller settling velocity (Dietrich, 1982; Kowalski *et al.*, 2016). The irregularity of the shape of MP disks leads to unsteady settling motions such as rotation, oscillation and tumbling, which also reduce *W* (Stringham *et al.*, 1969; Dietrich, 1982).

A few researchers (e.g., Dietrich, 1982; Camenen, 2007) proposed universal formulas for non-MP particles of various shapes considering shape effects, but these formulas do not apply to thin disks. For example, Dietrich (1982) proposed a formula (Eqn. 2.2) for particles of different shapes other than spheres considering *CSF* and *P*, but Eqn. (2.2) was valid for particles with *CSF* greater than 0.2, which is outside the range for disks and therefore it could not be applied to thin particle like MP disks. A second formula was developed for non-MP particles of various shapes, but it tends to underestimate the settling velocity of non-MP disks (Camenen, 2007). Similar conclusions of underestimation from Camenen's formula can be obtained from Figure 2.8 for both MP and non-MP disks (*Err* = - 80.9%). Note that the coefficients used in Camenen's formula were based on the MP disk characteristics of this study (*CSF* = 0.1, *P* = 3.0).

The existing $W^*$ - $D^*$ formulas for particles of various shapes do not show good agreement for disks (both MPs and non-MPs) due to the great shape difference of disks compared to spheres and sediments. Hence, a new model for both MP disks and non-MP disks was developed. A fourth-order polynomial model was proposed in this study to describe the correlation for disks:

$$\begin{aligned}\log(W^*) = &-6.333 + 4.223\log(D^*) - 0.923\log(D^*)^2 \\ &+0.102\log(D^*)^3 - 0.004\log(D^*)^4\end{aligned} \tag{2.17}$$

Coefficients of the formula were estimated by fitting MP disk data from this study, the 2D MP fragment data of Francalanci *et al.* (2021) and the data of non-MP disks from the literature (Stringham *et al.*, 1969; Hazzab *et al.*, 2008) (Stringham *et al.*, 1969; ha *et al.*, 2008; Song *et al.*, 2017), using the least-square method. The new formula presents a good fit to all the existing disk data with $R^2$ = 0.900 and *Err* = 15.5% (also see Figure 2.8). The p-value for T-test and F-

test is less than 0.001. The performance of Eqn. (2.18) shows an improvement in $W^*$ prediction for disk compared with existing formula of Camenen (2007) ($R^2$ = 0.420, *Err* = -80.9%).

Figure 2.9 shows that the drag coefficient, $C_D$, increases with the decrease of *Re.* In this study, when *Re* increases from 18.7 to 143.4, $C_D$ decreases from 7.9 to 2.5. MP and non-MP disks experience larger $C_D$ value than spheres with the same *Re* value. The formulas for spheres (Clift and Gauvin, 1971; Cheng, 2009) greatly underestimate $C_D$ values for disks. Many existing $C_D$ - *Re* formulas have been proposed considering shape effects for non-spherical particles as shown in Figure 2.9. A few of them give reasonable estimates of $C_D$ for both MP and non-MP disks, including those of Haider and Levenspiel (1989), Hölzer and Sommerfeld (2008) and Dioguardi *et al.* (2018). Since reasonable estimates have been achieved for MP disks, no efforts were made in this study to derive $C_D$ - *Re* formula specifically for MP disks.

Waldschläger and Schüttrumpf (2019) derived their $C_D$ - *Re* formula based on MPs with $0.1 < Re < 1 \times 10^4$. Only our data of MP disks and the data of 2D MP fragments from Francalanci *et al.* (2021) were used to compare with their formula. Although the formula of Waldschläger and Schüttrumpf (2019) for MP fragments considered *CSF*, it shows unsatisfactory accuracy (*Err* = 80.1%). Haider and Levenspiel (1989) as well as Dioguardi *et al.* (2018) introduced other shape descriptors such as sphericity and circularity in their formulas, and their formulas showed decent performance in prediction accuracy for MP and non-MP disk data (*Err* = 38.5% and 14.5%, respectively). Hölzer and Sommerfeld (2008) developed a formula that took the settling orientation into account. This formula presents improved accuracy with all disk data (MP and non-MP) with *Err* = – 1.71%. The improvement indicates that the settling orientation of disks along the trajectory impacts the $C_D$ - *Re* relationship and might need to be considered in future

studies.

2.4.4 Applicability to seawater and limitation of this study

This study examined MP disks settling in freshwater ($\rho$ = 998 kg/m$^3$), but the main results are expected to be applicable to seawater ($\rho$ = 1010 - 1030 kg/m$^3$), for example, the regime diagram of disks (Figure 2.3), the $D^*$ - $W^*$ equation of disks (Figure 2.8) and the $Re$ - $C_D$ relationship for disks (Figure 2.9). More specifically, in the regime diagram (Figure 2.3), the ambient fluid density and viscosity are taken into account in calculation of $Re_d$ and $I^*$. In the $D^*$ - $W^*$ equation (Figure 2.8), the dimensionless parameters $D^*$ and $W^*$ includes $\rho'$ ($\rho' = (\rho_s - \rho)/\rho$) and thus the ambient fluid density is considered, i.e., the equation (Eqn. 2.17) is still valid for seawater. In the $Re$ - $C_D$ diagram (Figure 2.9), the ambient fluid density and viscosity are also considered when calculating $Re$ and $C_D$, and therefore the diagram has been used for both freshwater and other fluids such as solutions of glycerin and rape oil (e.g., Komar an Reimers, 1978; Hölzer and Sommerfeld, 2008; Wang *et al.*, 2018).

The regime diagram considers different aspect ratio of disks; thus, it could be used to predict the settling trajectory for disks with various aspect ratios. However, the $D^*$ - $W^*$ and $Re$ - $C_D$ relationships were derived from MP disks with the aspect ratio of around 0.1. There could be some deviations in predicting $W^*$ and $C_D$ for MP disks with other aspect ratios, which is the limitation of this study and needs further investigations.

## 2.5 Conclusions

The knowledge on the settling of MP disks is scarce based on a comprehensive literature review. This study examined the settling behaviors of MP disks of three shapes with lengths $l$ from 1.5

- 5.0 mm. A detailed analysis was conducted of the settling trajectory and settling velocity, including their mean and instantaneous values. The diagram of the dimensionless moment of inertia $I^*$ versus disk Reynolds number $Re_d$ was expanded to predict the trajectories of MP disks. A new formula was proposed for the dimensionless terminal settling velocity $W^*$ for both MP and non-MP disks. The main conclusions are as follows:

- Three types of settling behaviors of MP disks were observed in this study. All MP disks with $l \leq 3$ mm and ABS disks with $l = 5$ mm fall steadily as a vertical line. PVC, PET and PC square disks with $l = 5$ mm oscillate during the falling; while PVC, PET and PC rectangular and triangular disks with $l = 5$ mm oscillate and rotate.

- For MP disks that fall steadily, their instantaneous horizontal settling velocity $W_y = 0$ and their instantaneous vertical settling velocity $W_x$ equals the mean terminal settling velocity $W$. For MP disks that have secondary motions, $W_x$ and $W_y$ oscillate periodically. The frequency and amplitude of the oscillation are related to the density and shape of MP disks.

- The shape, size, and density of MP disks affect the mean terminal settling velocity $W$. MP disks experience lower settling velocity than MPs of other shapes (e.g., sphere) at the same size $D_n$. The $W^*$ of disks could not be predicted by the $W^*$ - $D^*$ formulas developed for spheres and sediments. The new $W^*$ equation of this study shows good accuracy for disks with $R^2 = 0.900$ and $Err = 15.5\%$.

- The $C_D$ - $Re$ equation for spheres shows underestimation for MP and non-MP disks. But the existing $C_D$ - $Re$ relationships that take into account shape effect presented a reasonable approximation for disks, especially for the equation of Hölzer and Sommerfeld (2008),

which additionally considered the falling orientation of particles (*Err* = – 1.71%).

- The settling trajectory, velocity and drag coefficient of MPs would provide useful parameters in future modelling of MP fate. Moreover, the settling process of MPs is complicated in real aquatic environments and would be affected by factors including biofilm, sediment and the turbulence of flow, which needs to be further investigated.

**Table 2.1** Summary of experimental conditions on MP disks.

| Material | Number of disks | Length $l$, mm | Shape | Density $\rho_s$, kg/m$^3$ | Aspect ratio $h/l$ |
|---|---|---|---|---|---|
| PVC | 66 | 1.5, 3, 5 | square, rectangle, triangle | 1343 ± 5.0 | 0.07 – 0.10 |
| PET | 67 | 1.5, 3, 5 | square, rectangle, triangle | 1319 ± 5.0 | 0.08 – 0.15 |
| PC | 66 | 1.5, 3, 5 | square, rectangle, triangle | 1161 ± 5.0 | 0.10 – 0.17 |
| ABS | 29 | 5 | square, rectangle, triangle | 1038 ± 5.0 | 0.09 – 0.11 |

**Table 2.2** Mean terminal settling velocity (mm/s) and settling trajectory of disks. Velocity is mean ± standard deviation.

| Material | Shape | Length $l$, mm | Nominal diameter $D_n$, mm | Terminal settling velocity $W$, mm/s | Settling trajectory |
|---|---|---|---|---|---|
| PVC | square | 5 | 2.87 ± 0.02 | 46.36 ± 2.48 | zigzag |
| | | 3 | 1.66 ± 0.01 | 39.43 ± 0.45 | steady |
| | | 1.5 | 0.86 ± 0.01 | 23.25 ± 0.77 | steady |
| | rectangle | 5 | 2.27 ± 0.02 | 47.43 ± 1.15 | zigzag + transitional |
| | | 3 | 1.32 ± 0.01 | 35.5 ± 0.92 | steady |
| | triangle | 5 | 2.27 ± 0.02 | 44.23 ± 2.11 | zigzag + transitional |
| | | 3 | 1.32 ± 0.01 | 34.43 ± 0.81 | steady |
| PET | square | 5 | 2.66 ± 0.02 | 43.04 ± 1.19 | zigzag |
| | | 3 | 1.67 ± 0.02 | 38.93 ± 0.64 | steady |
| | | 1.5 | 0.94 ± 0.01 | 25.41 ± 0.56 | steady |
| | rectangle | 5 | 2.11 ± 0.01 | 44.54 ± 2.18 | zigzag + transitional |
| | | 3 | 1.33 ± 0.01 | 34.22 ± 1.1 | steady |
| | triangle | 5 | 2.11 ± 0.01 | 41.97 ± 1.97 | zigzag + transitional |
| | | 3 | 1.33 ± 0.01 | 33.35 ± 0.5 | steady |
| PC | square | 5 | 2.89 ± 0.02 | 38.51 ± 0.71 | zigzag |
| | | 3 | 1.75 ± 0.01 | 31.92 ± 0.33 | steady |
| | | 1.5 | 1.03 ± 0.00 | 23.76 ± 0.40 | steady |
| | rectangle | 5 | 2.29 ± 0.01 | 39.17 ± 0.44 | zigzag + transitional |
| | | 3 | 1.38 ± 0.01 | 28.45 ± 0.53 | steady |
| | triangle | 5 | 2.28 ± 0.01 | 35.56 ± 1.16 | zigzag + transitional |
| | | 3 | 1.39 ± 0.01 | 28.09 ± 0.97 | steady |
| ABS | square | 5 | 2.89 ± 0.01 | 23.76 ± 0.40 | steady |
| | rectangle | 5 | 2.29 ± 0.01 | 20.80 ± 0.45 | steady |
| | triangle | 5 | 2.29 ± 0.01 | 20.09 ± 0.46 | steady |

**Table 2.3** Instantaneous terminal settling velocities (minimum, maximum, amplitude and frequency) and the amplitude of trajectory of MP disks.

| | **Square disk** | | | **Rectangular disk** | | | **Triangular disk** | | |
|---|---|---|---|---|---|---|---|---|---|
| | **PVC** | **PET** | **PC** | **PVC** | **PET** | **PC** | **PVC** | **PET** | **PC** |
| $W_{x,max}$ (mm/s) | 62.3 ± 0.1 | 58.7 ± 0.1 | 46.9 ± 0.1 | 58.1 ± 0.1 | 53.0 ± 0.1 | 46.8 ± 0.1 | 57.1 ± 0.1 | 52.0 ± 0.1 | 43.7 ± 0.1 |
| $W_{x,\ min}$ (mm/s) | 35.3 ± 0.2 | 28.7 ± 0.1 | 31.2 ± 0.0 | 38.3 ± 0.1 | 37.7 ± 0.1 | 32.2 ± 0.1 | 37.6 ± 0.1 | 32.0 ± 0.1 | 25.2 ± 0.1 |
| $W_{y,\ max}$ (mm/s) | 35.2 ± 0.2 | 32.8 ± 0.1 | 15.4 ± 0.0 | 26.9 ± 0.1 | 22.8 ± 0.1 | 8.6 ± 0.1 | 25.7 ± 0.1 | 24.6 ± 0.1 | 16.8 ± 0.1 |
| Amplitude of $W_x$ (mm/s) | 13.5 ± 0.1 | 15.0 ± 0.1 | 7.9 ± 0.1 | 9.9 ± 0.1 | 7.7 ± 0.1 | 7.3 ± 0.1 | 9.8 ± 0.1 | 10.0 ± 0.1 | 9.3 ± 0.1 |
| Amplitude of $W_y$ (mm/s) | 35.2 ± 0.2 | 32.8 ± 0.1 | 15.4 ± 0.0 | 26.9 ± 0.1 | 22.8 ± 0.1 | 8.6 ± 0.1 | 25.7 ± 0.1 | 24.6 ± 0.1 | 16.8 ± 0.1 |
| Amplitude of trajectory (mm) | 2.1 ± 0.1 | 1.8 ± 0.1 | 1.4 ± 0.1 | 1.8 ± 0.1 | 1.5 ± 0.1 | 0.9 ± 0.1 | 1.7 ± 0.1 | 1.7 ± 0.1 | 1.4 ± 0.1 |
| Frequency $f_x$ (Hz) | 4.57 ± 0.27 | 4.40 ± 0.38 | 3.28 ± 0.27 | 4.56 ± 0.24 | 4.43 ± 0.24 | 2.91 ± 0.13 | 4.56 ± 0.30 | 4.40 ± 0.19 | 3.28 ± 0.14 |
| Frequency $f_y$ (Hz) | 2.27 ± 0.05 | 2.17 ± 0.06 | 1.67 ± 0.04 | 2.27 ± 0.06 | 2.22 ± 0.05 | 1.46 ± 0.02 | 2.26 ± 0.07 | 2.20 ± 0.07 | 1.67 ± 0.04 |

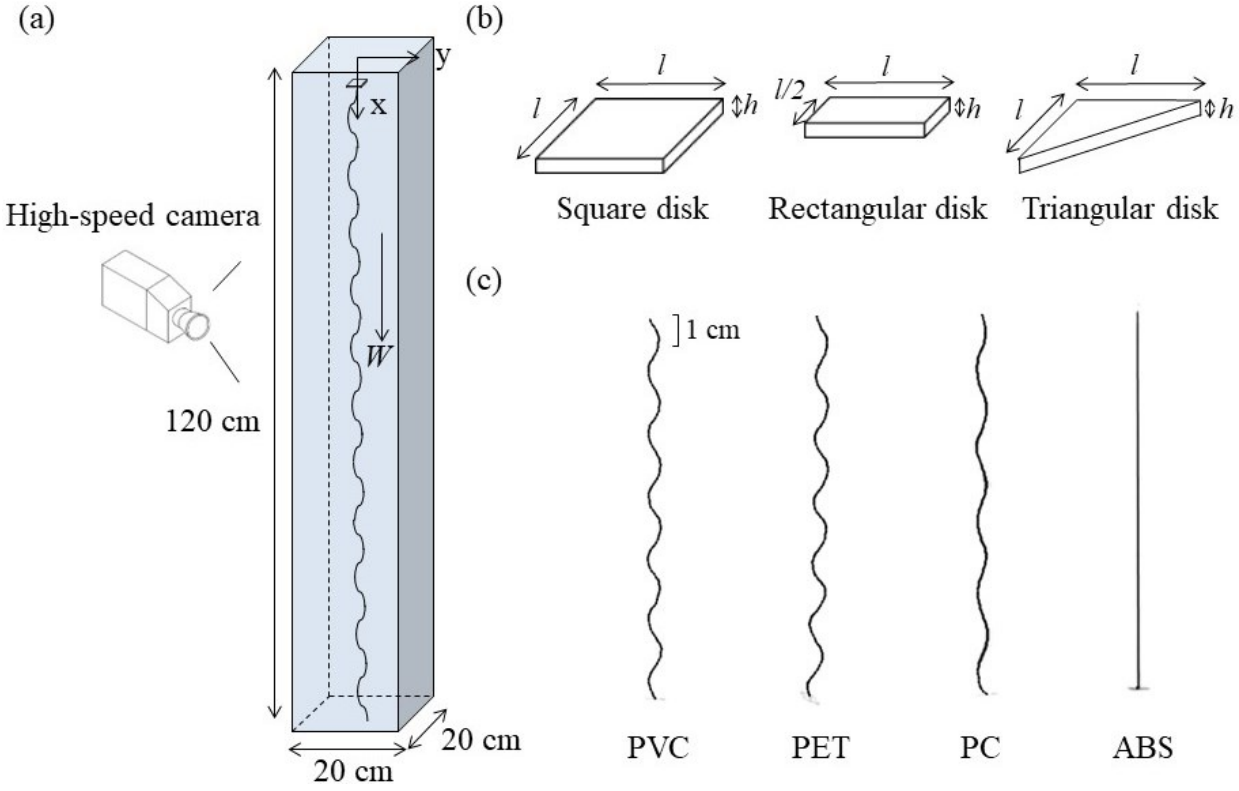


**Figure 2.1.** (a) Experimental setup, (b) shapes of MP disks, and (c) examples of settling trajectories of square disks ($l$ = 5 mm) of four MP materials. $l$ and $h$ are the length and thickness of an MP disk, respectively. The vertex angle of triangle MP disks is 90 degrees.

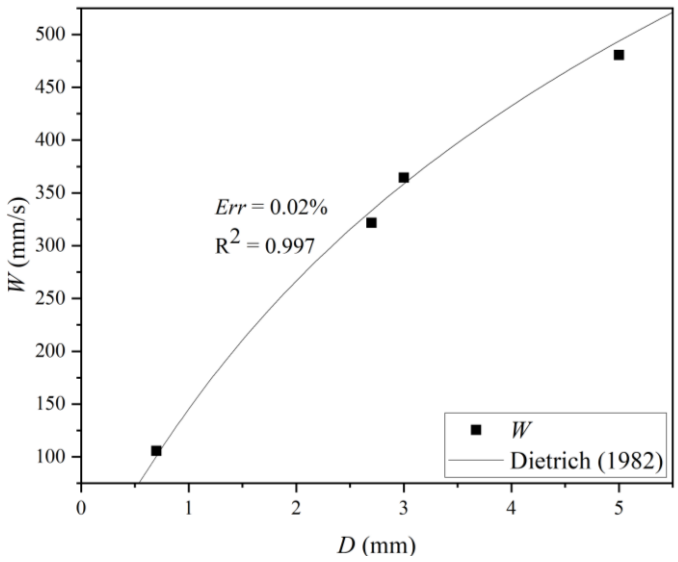


**Figure 2.2** Comparison of the measured terminal settling velocity $W$ of glass spheres ($\rho_s$ = 2.460 g/cm$^3$) of different diameters ($D$ = 0.7, 2.7, 3, and 5 mm) with the theoretical $W$ - $D$ relation for spherical particles (Dietrich,1982).

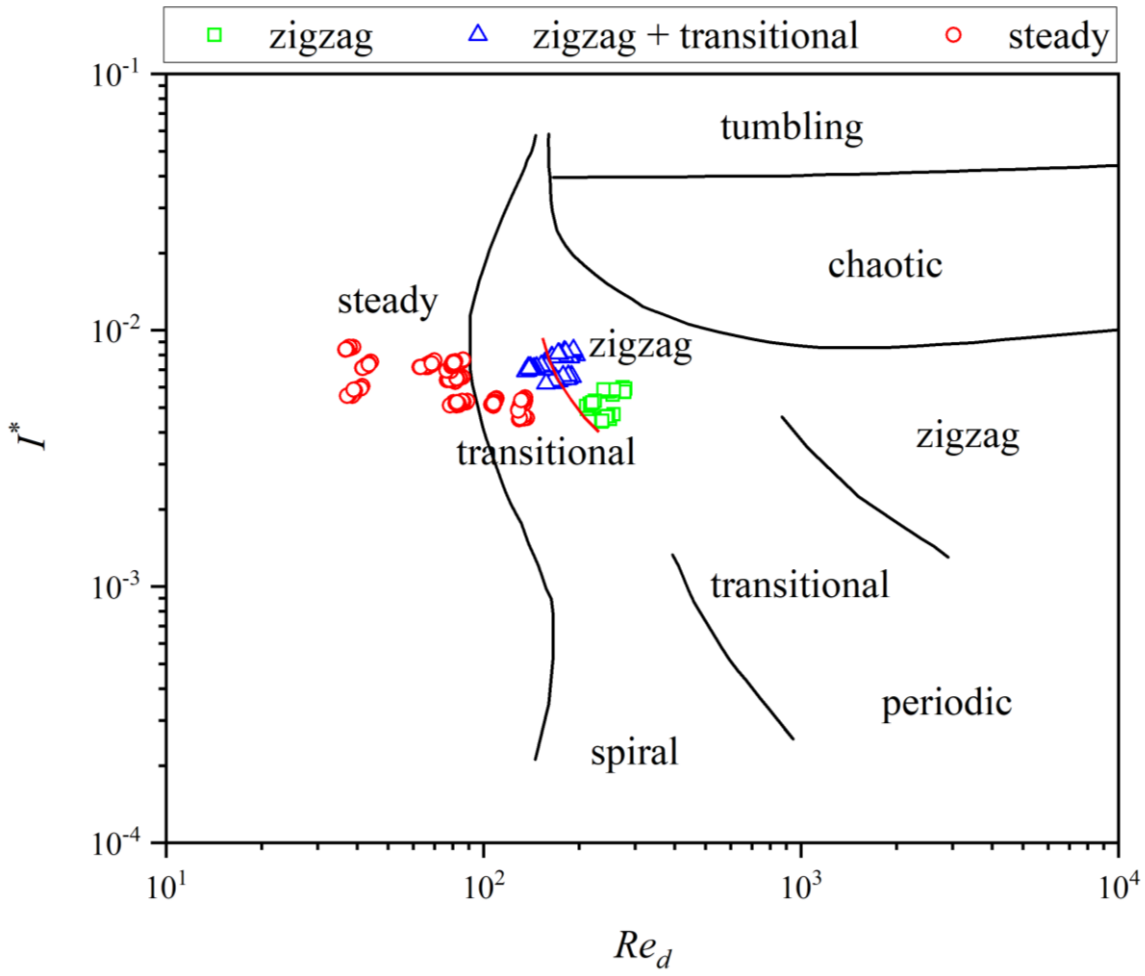


**Figure 2.3** Regime diagram of disk Reynolds number $Re_d$ versus dimensionless moment of inertia $I^*$. Black lines are the boundaries of regimes proposed by Field et al. (1997) and Zhong et al. (2011). The periodic regimes consist of the zigzag, transitional and spiral regimes. The red line is the proposed boundary between the zigzag regime and transitional regime according to this study.

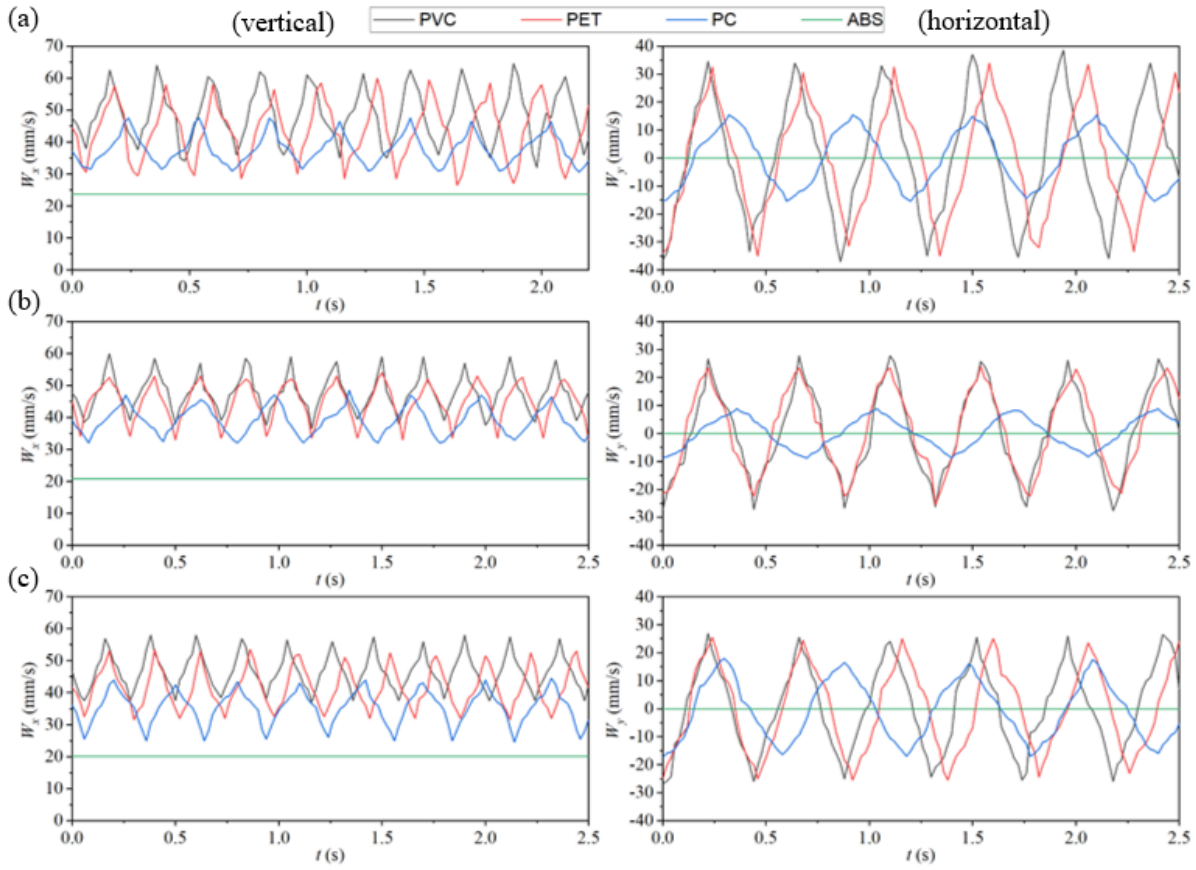


**Figure 2.4** Time evolution of instantaneous vertical settling velocity $W_x$ and horizontal settling velocity $W_y$ for MP disks (PVC, PET, PC and ABS) of different shapes: (a) square; (b) rectangle; and (c) triangle. MP disk $l$ = 5 mm.

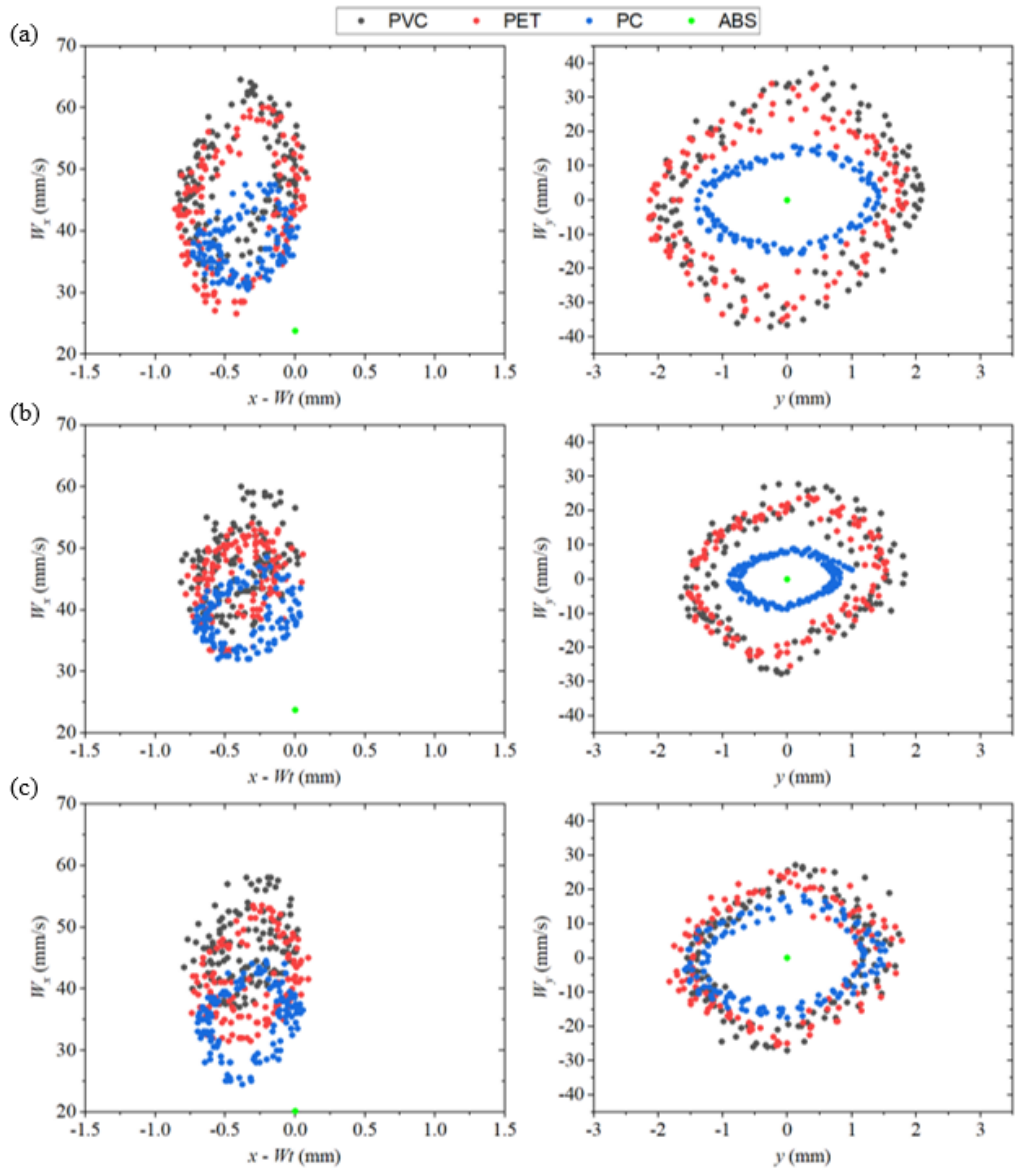


**Figure 2.5** Instantaneous vertical settling velocity $W_x$ and horizontal settling velocity $W_y$ versus distance $x$ - $Wt$ and $y$ for MP disks of different shapes: (a) square; (b) rectangle; and (c) triangle. MP disk $l$ = 5 mm.

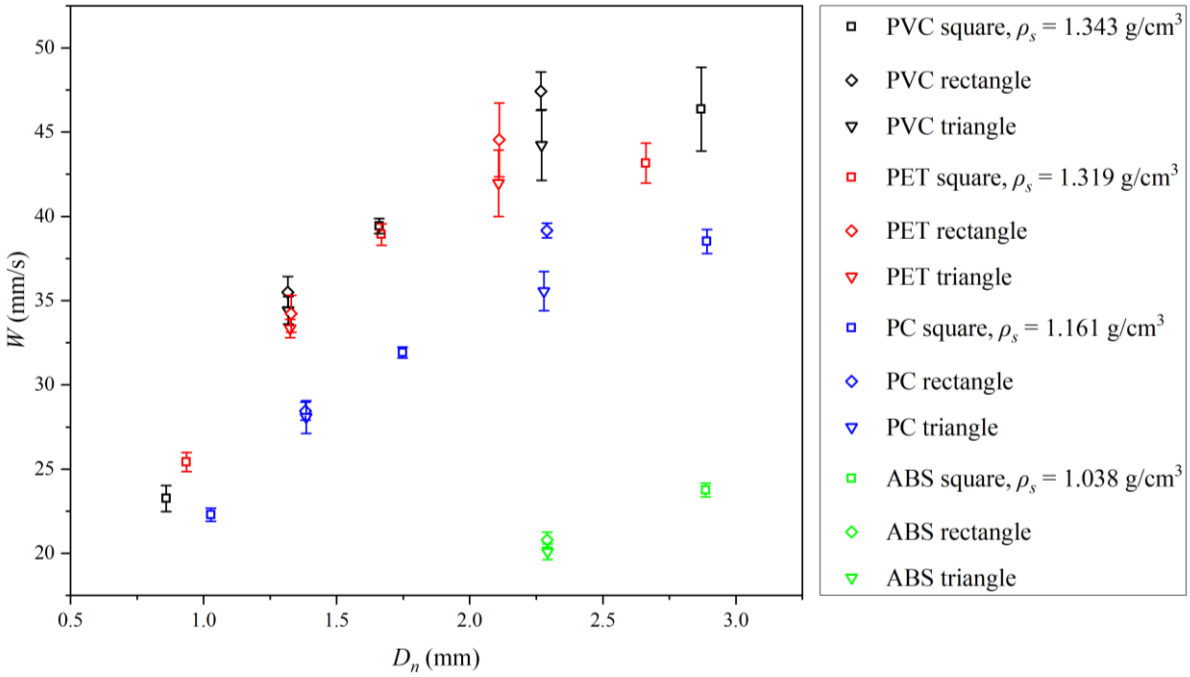


**Figure 2.6** Terminal settling velocity W of MP disks with different shapes (square, rectangular and triangular disk) and materials (ρs = 1.038 - 1.343 g/cm3) versus the nominal diameter Dn.

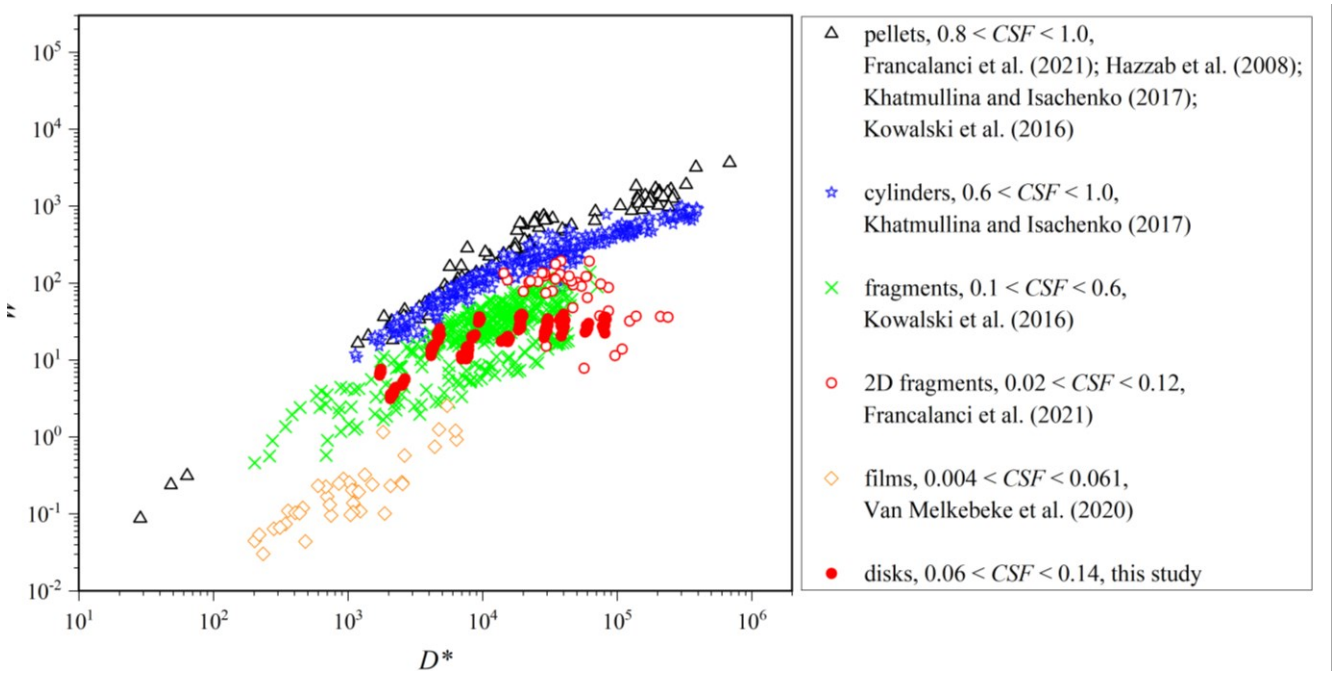


**Figure 2.7** Dimensionless settling velocity $W^*$ versus dimensionless particle diameter $D^*$ for MPs with different *CSF* ranges.

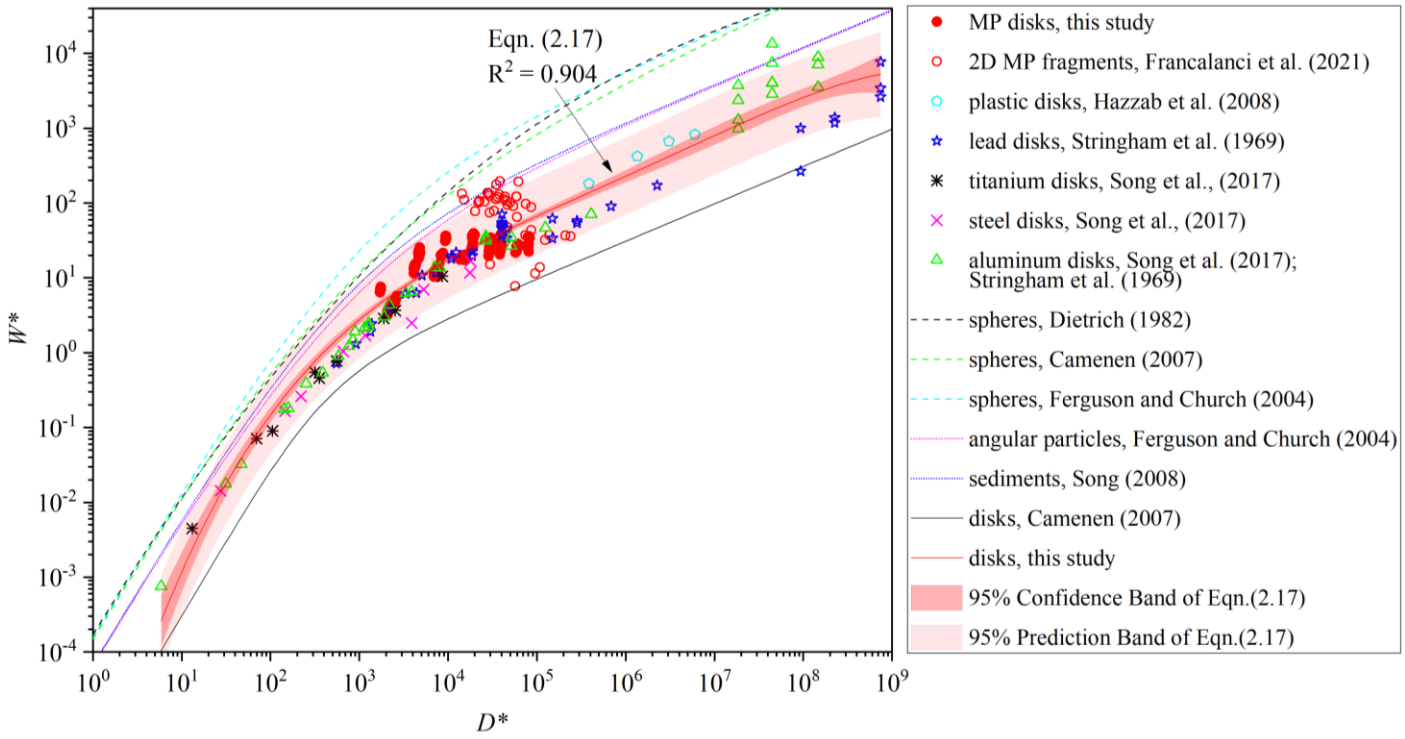


**Figure 2.8** Dimensionless settling velocity *W** versus dimensionless particle diameter *D** for MPs and non-MPs disks. The dots represent the experimental data collected from this study and the literature. The lines (except the red solid line) are formulas from the literature for non-MP particles shown for comparison purposes, including spheres, sediments and disks. The red solid line is the formula proposed in this study for disks (both MP and non-MP disks).

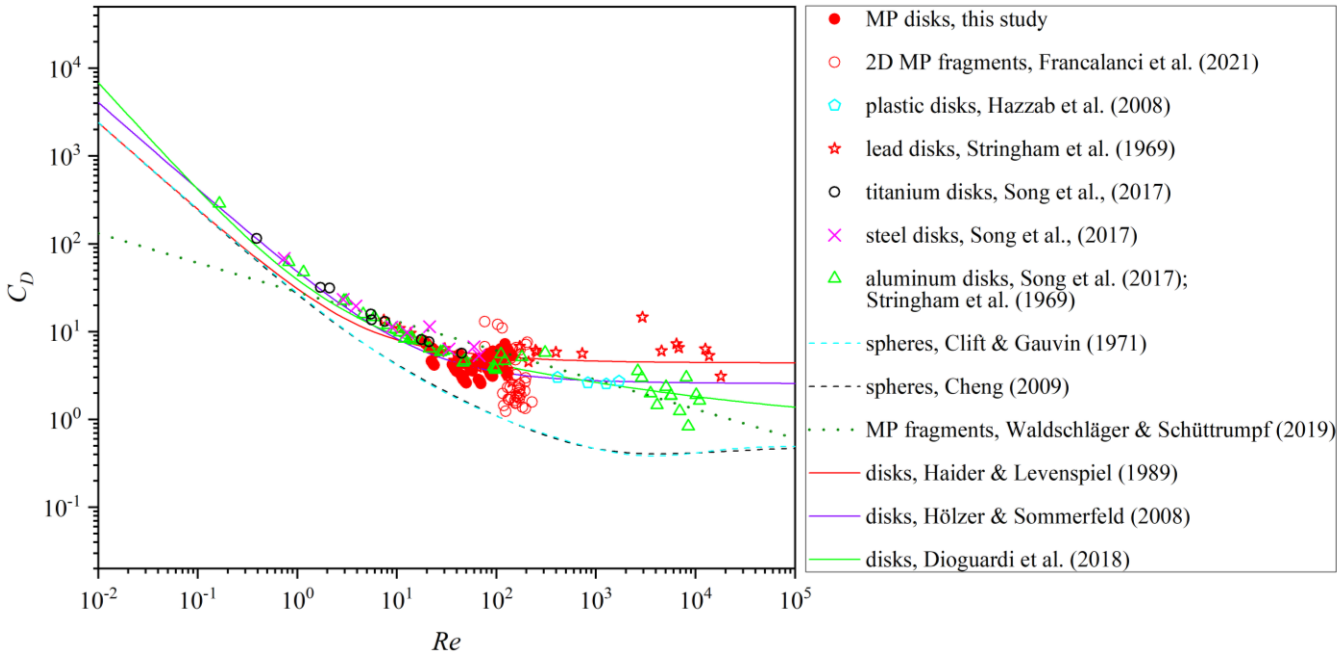


**Figure 2.9** Drag coefficient $C_D$ versus particle Reynolds number $Re$ for MP and non-MP disks. The dots are experimental data collected from this study and the literature. The lines are $C_D$-$Re$ relations from the literature for non-MP disks (metal disks, plastic disks and MP fragments).

## Chapter 3 Acceleration Fall of Microplastic Disks in Stagnant Water

### 3.1 Introduction

Microplastics (MPs) are usually defined as plastic particles less than 5 mm. They have been bringing increasing concerns in recent years because of their long-term durability and easy transport in the environment (Padervand *et al.*, 2020; Jalon-Rojas *et al.*, 2022). The aquatic environments receive the most MP pollution (Zhao *et al.*, 2019; Choi *et al.*, 2022). MPs are widespread in the water environments such as lakes, rivers, marine and Arctic ice (Free *et al.*, 2014; Obbard *et al.*, 2014; Yang *et al.*, 2015). MPs in the water environments threaten the aquatic biota as they can be directly ingested, which would cause obstruction concerns and reproduction issues (Yu *et al.*, 2022). Besides, MPs can absorb some contaminants such as persistent organics and metal (Guo and Wang, 2019). After ingestion, the toxicity of MP constituents and attached contaminants transfer and biomagnify in the food chains (Hidalgo-Ruz *et al.*, 2012; Yonkos *et al.*, 2014). MPs found in the marine have a wide range of physical properties including sizes, densities and shapes (Hidalgo-Ruz *et al.*, 2012; Khatmullina and Isachenko, 2017).

There are a great number of studies on the abundance, occurrence and influence of MPs in the water environment (Yu *et al.*, 2022). The hydrodynamic behaviors, however, are much less studied (Zhang, 2017). Over 90% of MPs in the marine accumulate in the sediment (Van Melkebeke *et al.*, 2020), which suggests the importance of the settling process. The terminal settling velocity is a significant hydrodynamic property to evaluate the possible pathway of MPs under the effect of currents and accumulated area, which is useful for the prediction of transport and fate of MPs in aquatic environments (Khatmullina and Chubarenko, 2019;

Francalanci *et al.*, 2021). There are some investigations focusing on the terminal settling process of MP pellets, fragments, disks and fibers, and it is concluded that the density, size and shape affect the terminal settling velocity of MPs (Ballent *et al.*, 2012; Bagaev *et al.*, 2017; Waldschläger and Schüttrumpf, 2019). According to Kowalski *et al.* (2016); Kaiser *et al.* (2019), the settling velocities of MPs with irregular forms were much lower than those of spheres with the same volume. Khatmullina and Isachenko (2017) indicated that existing formulas for the terminal settling velocity of sediments were appropriate for MP spheres and short cylinders, but exhibited a significant variation for MP long cylinders. Choi *et al.* (2022) tested the settling velocity and behaviors of MP fibers. Yang *et al*. (2022) reported three distinct settling trajectories of MP disks and indicted the settling velocity of MP disks is significantly lower than spheres of the same volume. The laboratory experiments show the MP disks and fibers do not always have the linear settling trajectory, and they have secondary motions such as oscillation and rotation during the falling (Choi *et al.*, 2022; Yang *et al.*, 2022).

However, up to now, researches about the settling process of MPs focus on the steady-state phase when MP particles fall at the terminal velocity. The accelerating phase before MPs reach the terminal velocity is always neglected and has not been investigated. The unsteady-state falling exists and cannot be ignored in some cases in real environments such as settling in the shallow water. Besides, the unsteady-state settling of particle is also related to some processes including gravity particle separation and particle classification because in those processes, figuring out the accelerating pathways of particle is necessary (Ferreira and Chhabra, 1998; Jalaal *et al.*, 2010). Only a few researches have investigated the accelerating phase of non-MP particles (Torabi and Yaghoobi, 2011; Jalaal *et al.*, 2012; Yaghoobi and Torabi, 2012; Yin *et al.*,

2017). These studies mainly focus on spherical and non-spherical particle with rectilinear settling trajectory and proposed the relationships of the instantaneous velocity, settling distance and time (Jalaal *et al.*, 2010; Torabi and Yaghoobi, 2011; Jalaal *et al.*, 2012; Yin *et al.*, 2017). The acceleration period of MPs has not been studied yet. Given the remarkable deviation in shape between disks and spheres, the acceleration period of MP disks might be different from that of spheres. Thus, a detailed study on unsteady-state phase of MP disks is imperative.

In this study, a laboratory experiment was conducted to study the acceleration phase of settling MP disks and investigate factors that influence the acceleration motion. We focus on the MP disks that are released in different ways. The settling trajectory and instantaneous velocity in both vertical and horizontal were analyzed. The relationships between the settling motion (including the settling distance and maximum settling velocity) and physical characteristics of MP disks (including the density, shape and size) were reported.

### 3.2 Theoretical Foundation

Consider an MP particle settling in water, the unsteady motion of the particle is given as (Choi *et al.*, 2022):

$$m_s \frac{d\overrightarrow{W}}{dt} = \overrightarrow{F_G} + \overrightarrow{F_B} + \overrightarrow{F_D} + \overrightarrow{F_L} + \overrightarrow{F_V} + \overrightarrow{F_P} + \overrightarrow{F_{Ba}} \tag{3.18}$$

where $m_s$ is the MP mass; $W$ and $t$ is the settling velocity and time of the MP particle. The forces acting on the MP particles are shown on the right-hand side, which denote gravity ($F_G$), buoyancy ($F_B$), drag force ($F_D$), lift force ($F_L$), virtual mass force ($F_V$), pressure gradient force ($F_P$) and Basset history force ($F_{Ba}$) in the water. The lift force ($F_L$) is divided into Magnus lift force and Staffman lift force. The Basset history force ($F_{Ba}$) is negligible when particle is larger

than 1μm and generally can be ignored for MPs (L. Li and Michaelides, 1992; Roy *et al.*, 2022). Besides, the ambient flow field is assumed not to be affected by the settling MPs (Choi *et al.*, 2022; Roy *et al.*, 2022), and thus, the ambient water velocity and pressure gradient force ($F_P$) is zero. Eqn. (1) is transformed to:

$$m_s \frac{d\vec{W}}{dt} = \overrightarrow{m_s g}(1-\frac{\rho_f}{\rho_s}) + \frac{1}{2} C_D \rho A_1 \vec{W}^2 + \frac{1}{2} C_L \rho A_2 \vec{W}^2 + \frac{1}{2} m_s \frac{\rho}{\rho_s} \frac{d\vec{W}}{dt} \tag{3.19}$$

where $\rho_s$ and $\rho$ is the density of MP particle and the ambient fluid, $g$ is the gravitational acceleration, $C_D$ and $C_L$ is the drag and lift coefficient, $A_1$ and $A_2$ is the particle projected area normal to the direction of the drag force ($F_D$) and lift force ($F_L$).

When the MP disk is not perpendicular to the direction of travel, $F_D$ is parallel to the direction of travel and $F_L$ is normal to the drag (Figure 3.1). As soon as the settling begins, the horizontal component of the resulting force causes the horizontal movement, the vertical component changes the vertical position (Stringham *et al.*, 1969). The equations of motion are as following (Stringham *et al.*, 1969):

$$\begin{aligned} m_s \frac{dW_x}{dt} &= m_s g(1-\frac{\rho_f}{\rho_s}) - \frac{1}{2} C_D \rho A_1 W_x^2 \cos\beta - \frac{1}{2} C_L \rho A_2 W_x^2 \sin\beta - \frac{1}{2} m_s \frac{\rho}{\rho_s} \frac{dW_x}{dt} \\ m_s \frac{dW_y}{dt} &= \frac{1}{2} C_D \rho A_1 W_y^2 \sin\beta - \frac{1}{2} C_L \rho A_2 W_y^2 \cos\beta \end{aligned} \tag{3.20}$$

Only very few studies have investigated the lift force on a non-spherical particle. It is generally assumed that the lift force is proportional to the drag force and related to the orientation of the non-spherical particle (Hoerner, 1965; Zastawny *et al.*, 2012), shown as Eqn. (4):

$$\frac{C_L}{C_D} = \sin^2\alpha \cos\alpha \tag{3.21}$$

## 3.3 Materials and Method

### 3.3.1 MP particles

MP disks in this study are cut from large plastic sheets made of polyvinyl chloride (PVC, $\rho_s$ = 1.343 g/cm$^3$), polycarbonate (PC, $\rho_s$ = 1.161 g/cm$^3$), and acrylonitrile butadiene styrene (ABS, $\rho_s$ = 1.038 g/cm$^3$). These plastic sheets are ordered online. PVC, PC and ABS are common materials for plastic production and waste in environment, for example, PVC is widely used in pipes and shower curtains; PC is used for construction materials; and ABS for the raw materials for some monitors and keyboards (Andrady, 2011; W. C. Li *et al.*, 2016; Waldschläger and Schüttrumpf, 2019). Each plastic sheet was cut into MP disks of three shapes - square, rectangle, and triangle (Figure 3.1). According to Yang *et al*. (2022), the MP disks with side lengths $l$ = 3.0 and 5.0 mm has totally different terminal trajectory, and thus the MP disks with side lengths $l$ = 3.0 and 5.0 mm are used in this study to investigate the size effects on acceleration phase. The aspect ratio $h/l$ is 0.1 ($h$ represents the thicknesses of disks). The length and thickness were measured with a digital caliper (± 0.001 mm accuracy).

The MP density was measured using the method based on ISO 1183-1 (2012) and the measured density was checked with the density values provided from the online MP dealers. The MP disks were placed into a beaker with 100 ml of distilled water. After MP disks had sunk to the bottom, the zinc chloride solution ($\rho$ = 1.600 g/cm$^3$) was added to the beaker by a burette. the solution was stirred after each addition. The zinc chloride solution is added and mixed until the MP disks stay suspended for at least 1 min. The density of the solution was determined by weighing 1 ml solution by an analytical balance (± 0.001 g accuracy) (1 ml solution is delivered by an automatic pipette). The MP density is equal to the density of the solution.

### 3.3.2 Experiment setup and procedure

The experimental setup is shown in Figure 3.2(a): the settling column is made of plexiglass with a square cross-section of 20 × 20 cm and a height of 120 cm. The column was filled with tap water and the water temperature is kept at 20 ± 0.5 °C. Dotted markers were made on the centroid of the disk surface on each side. Before starting the settling experiment, MP disks were submerged in the experimental water for three hours to minimize the static surface charge. Each MP disk was placed in the center of the column by tweezers and released at 7 cm below the water surface to prevent surface tension. The disks fell freely with the initial velocity of zero. After 30 cm settling, all MP disks reach terminal velocity. As the focus of this study is the acceleration phase, 30 cm of the falling height from releasing was recorded using a high-speed camera (Phantom v211, USA) at a frame rate of 100 fps and a resolution of 1280 × 720 pixels.

Three release angles (0°, 45° and 90°) were tested in the experiment. For MP disks of each density, size and shape with the release angle of 0°, the disks were directly released in horizontal position (Figure 3.3(a)). For each MP disk set with the release angle of 45° and 90°, they were released in five ways (Case 1 - Case 5) (Figure 3.3(b)). The disk with release angle of 0° and 90° was directly dropped by tweezers. A plexiglass slope with vertex angle of 45°was attached to the wall of settling column. MP disk with the release angle of 45° was released at the release point (Figure 3.2(b)).

The settling trajectory of MP disks was determined by connecting the dots marked on centroid of the disk using software *ImageJ* (National Institutes of Health, USA). The *x*-direction was the vertically downward direction; the *y*-direction was the horizontal direction (shown in Figure 3.2(a)). $W_x$ and $W_y$ is the instantaneous settling velocities in the *x* and *y* directions, which were

calculated from processing the images every 0.02 s after releasing disks. The calculated drag coefficient from different methods is compared and shown in form of the absolute value of relative error (|*Err*|) in this study:

$$|Err| = \frac{1}{N}\sum \frac{\left|C_D - C_D{}'\right|}{C_D} \tag{3.22}$$

**3.4 Results and discussion**

3.4.1 Settling trajectory

The settling trajectory of MP disks in the acceleration phase is different from that in the terminal period. The MP disk with the release angle of 0° starts to zigzag immediately with smaller oscillation (compared with terminal phase) after releasing, which indicates $L_x$ and $L_y$ is zero. The MP disks with the release angles of 45° and 90° firstly adjust to the position where the plane of disk face is horizontal and then fall (Figure 3.3(d)). The distance from the release point to the place where the MP disk first reaches the horizontal position is defined as the adjustment distance.

The settling trajectory in the adjustment period of MP disk with the release angle of 45° and 90° is shown in Figure 3.4. MP disks with angle of 45°and 90° show distinct adjustment trajectory. The settling trajectory for disk of 45° is almost linear, while that for disk of 90° is a curve. The angle between the line from the start to the end of the adjustment period and vertical plane is defined as γ (Figure 3.2(a)). γ grows with the release angle decreasing. For MP disks of 45° is 35° ± 5° and γ for MP disks of 90° is 17° ± 3°. According to the settling trajectory, the adjustment distance in the horizontal ($L_x$) and vertical ($L_y$) directions was obtained.

In Figure 3.4, it is shown that the settling trajectory is affected by the MP density, size, and release angle. $L_x$ for MP disk with the release angle of 90° is much larger than that with angle of 45°; $L_x$ for angle of 90° is twice of that for angle of 45°. Besides, with the decrease in density from 1.343 g/cm$^3$ (PVC) to 1.038 g/cm$^3$ (ABS), $L_x$ decreases by 25% for the release angle of both 90° and 45°. In comparison of two MP disks of lengths $l$ of 3 mm and 5 mm, 5mm disks have 47% larger $L_x$ than 3 mm disks. $L_x$ and $L_y$ were summarized in Table 3.2 and Table 3.3. Comparing the results of Case 2 and Case 3, the other factors influence $L_x$ and $L_y$ can be concluded. For example, $L_x$ of Case 2 is 50% larger than $L_x$ of Case 3 and it indicates that the area of MP disks perpendicular to the motion has an influence on $L_x$. A dimensionless value named crosswise sphericity ($\Phi_\perp$) was used herein to describe the area of MP disks perpendicular to the motion. $\Phi_\perp$ denotes the ratio of the cross-section area of the volume equivalent sphere to the projected cross-sectional area of the particles perpendicular to the motion (Hölzer and Sommerfeld, 2008). The result obtained by comparison of Case 2 and Case 3 shows that with the larger $\Phi_\perp$, $L_x$ becomes smaller. Comparing results of Case 3 and Case 4, in which MP has the same $\Phi_\perp$, it is shown that MP shape exerts an impact on $L_x$. The Corey shape factor (*CSF*) is used to describe the difference in shape. *CSF* is a common factor describing the shape of particle. $CSF = c/\sqrt{ab}$, where $a$, $b$ and $c$ are the longest, intermediate and shortest lengths of the particle in three perpendicular axes (Khatmullina and Isachenko, 2017; Francalanci *et al.*, 2021). The impact of MP density, size and release angle was analyzed in the dimensionless form of $\Delta\rho$, $D^*$ and $\theta$ (in radian). $\Delta\rho = (\rho_s - \rho)/\rho$ and $D^* = gD_n/v^2$, where $D_n$ is the nominal diameter, which is the diameter of a sphere that has the same volume as the MP disk; $v$ is the kinematic viscosity of the fluid (Dietrich, 1982). $L_y$ can be analyzed in

the same way as $L_x$. Figure 3.4 shows the dependence of $L_x$ and $L_y$ on the impact factors including $\theta, \Delta\rho, \Phi_\perp, D^*$ and *CSF*. The power of each factor is determined using software *Origin 2019*. Note that $L_x$ and $L_y$ for horizontal release ($\theta = 0$) disks are 0. Linear regression was applied to the analysis and has the coefficient of determination $R^2$ of 0.761 and 0.753 for $L_x$ and $L_y$, respectively. No comparison of the impact factors for $L_x$ and $L_y$ was conducted because up to now, no studies have focused on the adjustment phase of particles.

### 3.4.2 Instantaneous settling velocity

To investigate effects of MP particle properties on MP settling behaviors in the acceleration period, the instantaneous settling velocity in both vertical ($W_x$) and horizontal ($W_y$) directions were calculated based on the trajectory (Figure 3.6 and Figure 3.7). The settling velocity of MP disks with the release angles of 0° gradually grows with oscillation from 0 to the terminal settling velocity. While MP disks with the release angles of 90° and 45° experience an enormous acceleration to the maximum values ($W_{x,max}$ and $W_{y,max}$) and deceleration in the adjustment phase. After the adjustment phase MPs start zigzagging and accelerating to terminal velocity. The acceleration period of MP disks is short and MP disks reach the terminal velocity within 1.5 s. The settling velocity of disks in acceleration phase is not compared and discussed with other studies since up to now, no research on the topic has been reported.

The density, size, release angle and release way affect the settling velocity of MP particles in adjustment phase. For instance, in Case 1, MP disks with the release angle of 90° have 22% higher $W_{x,max}$ and $W_{y,max}$ as well as longer adjustment time $T$ than disks with 45°. In comparison of disks of different density such as PVC disks and ABS disks, the disks with larger density have 60% higher $W_{x,max}$ and $W_{y,max}$. For disks of the same material, but with different lengths $l$

of 3 mm and 5 mm in Case 1, the ones with $l = 5$ mm have larger $W_{x,max}$, $W_{y,max}$ and $T$. Moreover, the differences in $W_{x,max}$, $W_{y,max}$ and $T$ indicate the effects of release ways on the adjustment phase, which is related to $CSF$ and $\Phi_{\perp}$. $W_{x,max}$ and $W_{x,max}/W_{x,terminal}$ ($W_{x,terminal}$ is the mean settling velocity) also show a linear relationship with the same impact factors as $L_x$ and $L_y$ ($\theta$, $\Delta\rho$, $D^*$, $CSF$ and $\Phi_{\perp}$) (Figure 3.8). Only disks that have adjustment phase are considered here (i.e., disks with the release angles of 90° and 45°). As shown in Figure 3.8, both $W_{x,max}$ and $W_{x,max}/W_{x,terminal}$ are in proportion to $\theta$, $\Delta\rho$, $D^*$ and $\Phi_{\perp}$, but are inversely proportional to $CSF$. The relationship of $W_{x,max}$ on the impact factors shows a worse linear fit with $R^2 = 0.729$ than $W_{x,max}/W_{x,terminal}$ ($R^2 = 0.732$).

3.4.3 Drag coefficient

When MP disks settle from stationary, the settling velocity changes with time and the drag coefficient of particle also change with time. In the adjustment phase, the forces exerted on the MP disk are not only vertical. They have horizontal component which drive the disk having lateral drift. The drag force on the MP disk is a dynamic situation and changes with time. Based on the motion of MP disk in vertical direction in Eqn. (3), drag coefficient $C_D$ of MP disks is calculated as following:

$$C_D = \frac{2V}{(A_1 \cos\beta + A_2 \sin^2\alpha \cos\alpha \sin\beta) W_y^{\,2}} \left[ g\left(\frac{\rho_s}{\rho} - 1\right) - \frac{dW_y}{dt}\left(\frac{\rho_s}{\rho} + \frac{1}{2}\right) \right] \qquad (3.23)$$

According to Figure 3.1, $A_1 = A\cos\alpha$ and $A_2 = A\sin\alpha$, where $A$ is the area of the disk face and $V$ is the volume of the MP disk.

In some studies about the acceleration phase of non-spherical, non-MP particles, the particles were regarded as spheres, using nominal diameter $D_n$ when describing the motion of non-

spherical particles (Jalaal *et al.*, 2012; Yaghoobi and Torabi, 2012). If the MP disk is regarded as a volume equivalent sphere, drag coefficient $C_D'$ of MP disks is calculated by:

$$m_s \frac{dW}{dt} = m_s g(1-\frac{\rho_f}{\rho_s}) - \frac{1}{8}\pi D_n^2 C_D' \rho W^2 - \frac{1}{2} m_s \frac{\rho}{\rho_s} \frac{dW}{dt} \tag{3.24}$$

The absolute value of relative error ($|Err|$) was used to compare the drag coefficient of MP disks calculated by Eqn. (6) and Eqn. (7).

For the PVC square disk with the release angle of 90°, the comparison of drag coefficient between two equations (the square and cross in Figure 3.8) shows enormous difference with $|Err| = 251.9\%$. It is unreasonable to consider the MP disk as a sphere due to the non-negligible deviation. Thus, Eqn. (6) is used to calculate drag coefficient $C_D$ of MP disks.

Figure 3.8 exhibits the time evolution of $C_D$ for MP disks in Case 1 with the release angles of 90° and 45°. In the adjustment phase, when MP disks begin to fall, the settling velocity is close to 0 and $C_D$ is infinite. Then, $C_D$ starts to decrease and stay at a low value $C_{D,min}$. At the end of the adjustment phase, $C_D$ increases. The results show $C_{D,min}$ is influenced by the release angle and size, but not related to the MP density. 5 mm PVC, PC and ABS disks with the release angle of 90° have similar $C_{D,min}$ values around 0.2, while disks with $l$ = 3 mm or release angle of 45° have larger $C_{D,min}$. The time $t_{min}$ for $C_D$ stable at $C_{D,min}$ is related to size, density and release angle. $t_{min}$ for the disk of $l$ = 3 mm is significantly smaller than that for $l$ = 5 mm. In comparison of the same disk but with different release angle, $t_{min}$ for disk with the release angle of 90° is larger than that of 45°. When considering the influence of density, the PVC disk has the shortest $t_{min}$ and ABS disk has the longest. It is indicated that the MP disk with the larger density has the shorter $t_{min}$.

### 3.5 Conclusion

In this study, MP disks of three polymer types were released into the water by different ways. Due to the significant deviation in shape, MP disks have different acceleration motions from spheres. After releasing from the release point, MP disks firstly adjust to the horizontal position and accelerate to terminal velocity. Not only vertical sedimentation but also lateral drift was observed in the experiment.

The settling trajectory and instantaneous velocity in vertical and horizontal directions are analyzed in details. During the adjustment phase, the MP disks have a sharp acceleration at first and then have a deceleration. Results indicated that the adjustment distance $L_x$ and $L_y$, maximum vertical settling velocity $W_{x,max}$ as well as $W_{x,max}/W_{x,terminal}$ are in correlation to $\theta$, $\Delta\rho$, $\Phi_{\perp}$, $D^*$ and in reverse correlation to $CSF$. The MP disk has non-linear settling trajectory in the adjustment phase because the resultant force acting on the MP disk is not directly vertical. There is significant deviation ($|Err|$ = 251.9%) in drag coefficient ($C_D$) estimation when the model of acceleration motions of spheres is applied to MP disks. According to the new equation in this study, it is indicated that $C_D$ firstly decreases to a low value and then increases in the adjustment phase and it is affected by density, size and release angle.

Up to date, little is known about the motion of MP particles before they reach the terminal velocity. The future work about the unsteady motion of MPs of other shapes such as cylinders, fibers and fragments in acceleration phase is needed.

**Table 3.1** Summary of experimental conditions on MP disks.

| Material | Length $l$, mm | Shape | Release angle $\theta$ | Density $\rho_s$, kg/m$^3$ | Aspect ratio $h/l$ | $CSF$ |
|---|---|---|---|---|---|---|
| PVC | 3, 5 | square, rectangle, triangle | 0°, 45°, 90° | 1343 ± 5.0 | 0.10 | 0.10 |
| PC | 3, 5 | square, rectangle, triangle | 0°, 45°, 90° | 1161 ± 5.0 | 0.10 | 0.14 |
| ABS | 5 | square, rectangle, triangle | 0°, 45°, 90° | 1038 ± 5.0 | 0.10 | 0.08 |

**Table 3.2** Adjustment distance (mm) of MP disks with the release angle of 90° in the (a) vertical ($L_x$) and (b) horizontal ($L_y$) directions. The adjustment distance is mean ± standard deviation.

(a)

| $L_x$ | **PVC, $l$ = 5 mm** | **PC, $l$ = 5 mm** | **ABS, $l$ = 3 mm** | **PVC, $l$ = 3 mm** | **PC, $l$ = 3 mm** |
|---|---|---|---|---|---|
| Case 1 | 3.78±0.60 | 3.23±0.78 | 2.58±0.37 | 1.55±0.27 | 1.33±0.48 |
| Case 2 | 2.22±0.31 | 2.05 ± 0.33 | 1.79±0.23 | 1.31±0.29 | 1.08±0.25 |
| Case 3 | 0.87±0.11 | 0.82±0.15 | 0.78±0.14 | 0.76±0.23 | 0.46±0.09 |
| Case 4 | 1.55±0.4 | 1.38±0.49 | 1.36±0.28 | 1.35±0.32 | 1.17±0.25 |
| Case 5 | 1.37±0.34 | 1.35±0.26 | 1.09±0.22 | 0.60±0.19 | 0.56±0.20 |

(b)

| $L_y$ | **PVC, $l$ = 5 mm** | **PC, $l$ = 5 mm** | **ABS, $l$ = 3 mm** | **PVC, $l$ = 3 mm** | **PC, $l$ = 3 mm** |
|---|---|---|---|---|---|
| Case 1 | 1.44 ± 0.17 | 1.24 ± 0.15 | 0.78 ± 0.29 | 0.46 ± 0.05 | 0.43 ± 0.07 |
| Case 2 | 0.95 ± 0.11 | 0.75 ± 0.33 | 0.42 ± 0.13 | 0.29 ± 0.07 | 0.29 ± 0.10 |
| Case 3 | 0.31 ± 0.04 | 0.33 ± 0.05 | 0.29 ± 0.05 | 0.21 ± 0.05 | 0.16 ± 0.01 |
| Case 4 | 0.54 ± 0.08 | 0.54 ± 0.18 | 0.46 ± 0.13 | 0.25 ± 0.03 | 0.26 ± 0.02 |
| Case 5 | 0.34 ± 0.14 | 0.29 ± 0.07 | 0.22 ± 0.06 | 0.19 ± 0.05 | 0.17 ± 0.12 |

**Table 3.3** Adjustment distance (mm) of MP disks with the release angle of 45° in the (a) vertical ($L_x$) and (b) horizontal ($L_y$) directions. The adjustment distance is mean ± standard deviation.

(a)

| $L_x$ | PVC, $l$ = 5 mm | PC, $l$ = 5 mm | ABS, $l$ = 3 mm | PVC, $l$ = 3 mm | PC, $l$ = 3 mm |
|---|---|---|---|---|---|
| Case 1 | 1.25±0.08 | 1.13±0.11 | 1.02 ± 0.13 | 0.72 ± 0.11 | 0.65±0.06 |
| Case 2 | 1.18±0.05 | 1.15±0.05 | 1.09 ± 0.22 | 0.88 ± 0.04 | 0.78 ± 0.04 |
| Case 3 | 0.86±0.26 | 0.63±0.14 | 0.56±0.16 | 0.53±0.05 | 0.32±0.03 |
| Case 4 | 1.09±0.23 | 0.86±0.12 | 0.87±0.18 | 0.75±0.15 | 0.67±0.12 |
| Case 5 | 1.05±0.13 | 0.85±0.15 | 0.84±0.22 | 0.72±0.15 | 0.69±0.04 |

(b)

| $L_y$ | PVC, $l$ = 5 mm | PC, $l$ = 5 mm | ABS, $l$ = 3 mm | PVC, $l$ = 3 mm | PC, $l$ = 3 mm |
|---|---|---|---|---|---|
| Case 1 | 1.21 ± 0.11 | 1.08 ± 0.11 | 0.74 ± 0.05 | 0.52 ± 0.03 | 0.49 ± 0.04 |
| Case 2 | 0.91 ± 0.05 | 0.94 ± 0.4 | 0.67 ± 0.14 | 0.55 ± 0.02 | 0.51 ± 0.04 |
| Case 3 | 0.59 ± 0.17 | 0.46 ± 0.13 | 0.38 ± 0.13 | 0.40 ± 0.05 | 0.32 ± 0.03 |
| Case 4 | 0.83 ± 0.13 | 0.79 ± 0.10 | 0.47 ± 0.11 | 0.48 ± 0.06 | 0.34 ± 0.04 |
| Case 5 | 0.83 ± 0.19 | 0.64 ± 0.12 | 0.34 ± 0.10 | 0.42 ± 0.09 | 0.37 ± 0.01 |

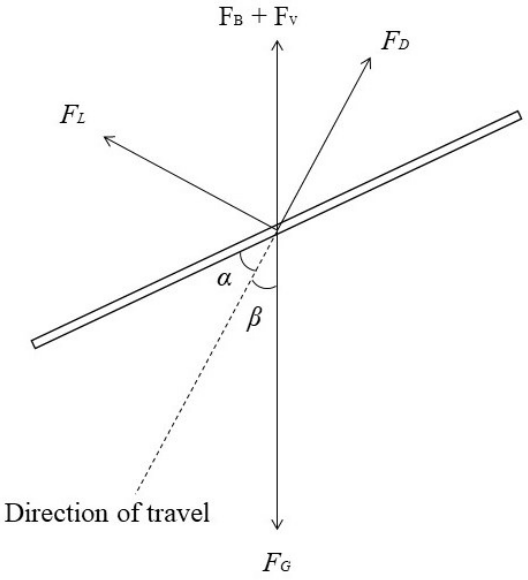


**Figure 3.1** Forces on the settling disk. $F_G$, $F_B$, $F_D$, $F_L$ and $F_V$ denote gravity, buoyancy, drag, lift and virtual mass forces, respectively. α is the angle between the plane of the disk face and the direction of travel. β is the angle between the direction of travel and the vertical plane.

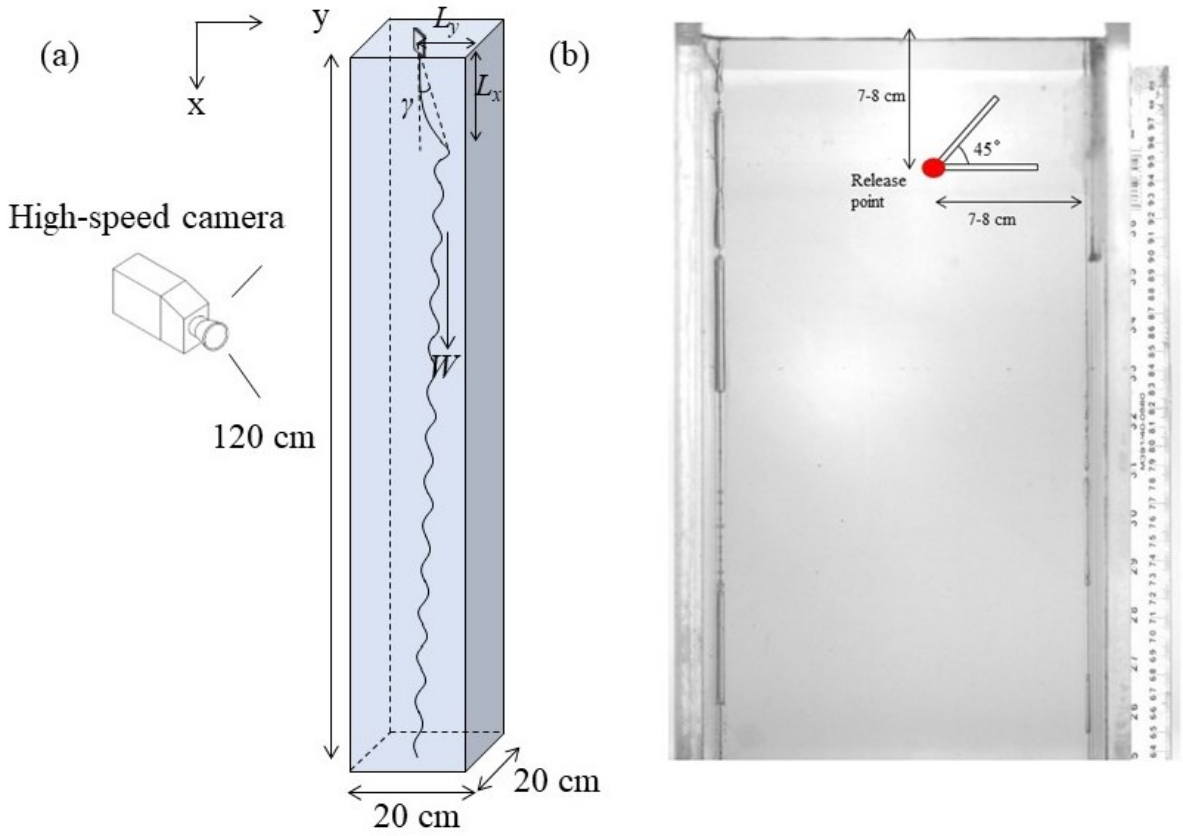


**Figure 3.2** Scheme of (a) Experimental setup and (b) attached slope on the settling column for disk releasing.

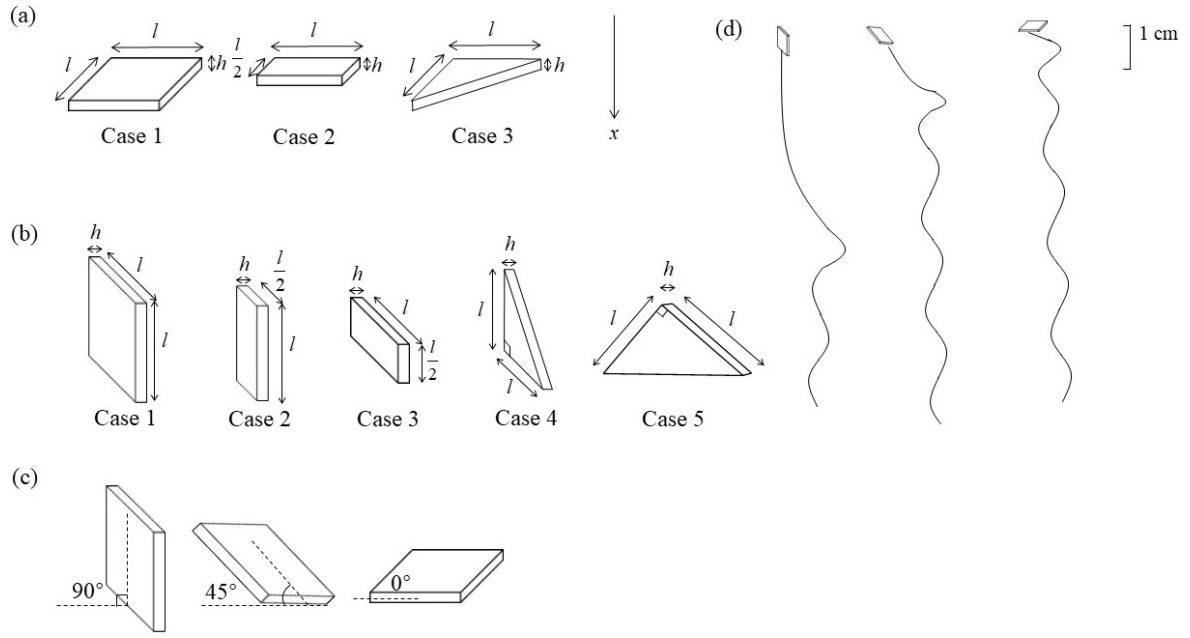


**Figure 3.3** (a) three release ways of MP disks with release angles of 0°, (b) five release ways of MP disks with release angles of 45° and 90°, (c) three release angles, and (d) examples of settling trajectories of square disks with release angles of 90°, 45° and 0°. *l* and *h* are the length and thickness of an MP disk, respectively. The vertex angle of triangle MP disks is 90°.

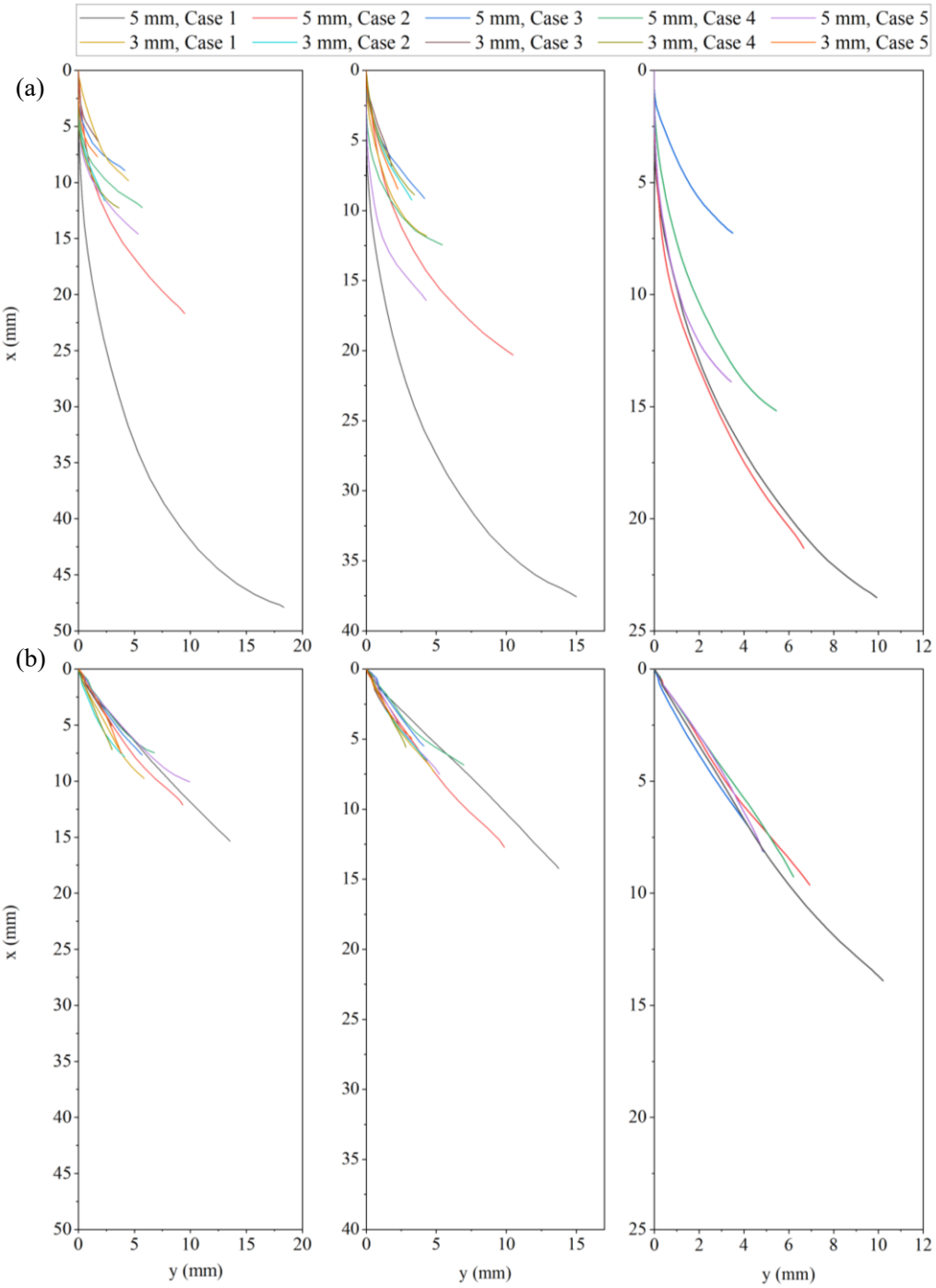


**Figure 3.4** Settling trajectory of MP disk (PVC, PC and ABS) in the adjustment phase with the initial release angle of (a) 90° and (b) 45°.

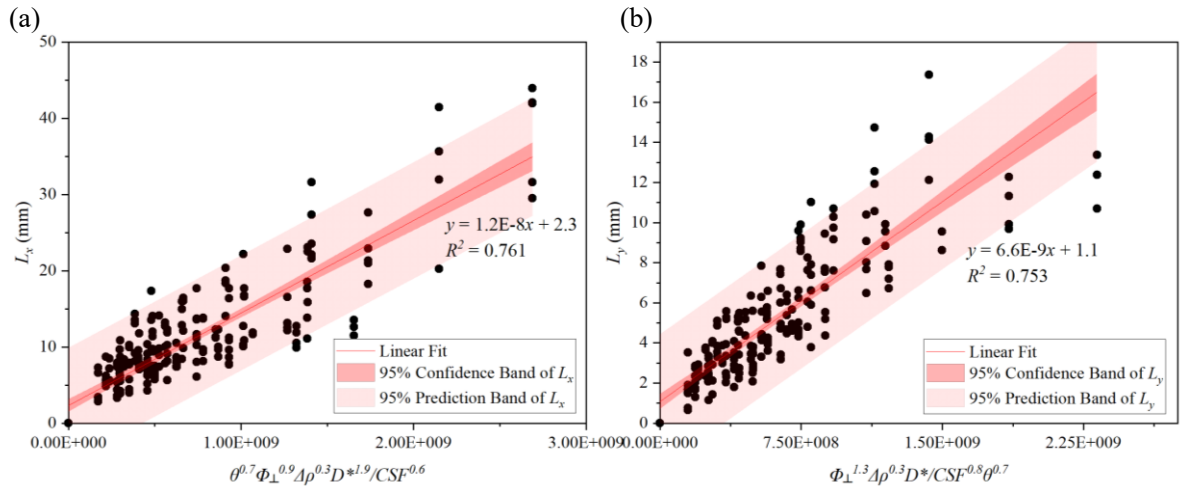


**Figure 3.5** Adjustment distance of MP disk (PVC, PC and ABS) in (a) vertical direction and (b) horizontal direction, released in five ways (Case 1 - Case 5) with the release angle of 90°, 45° and 0°.

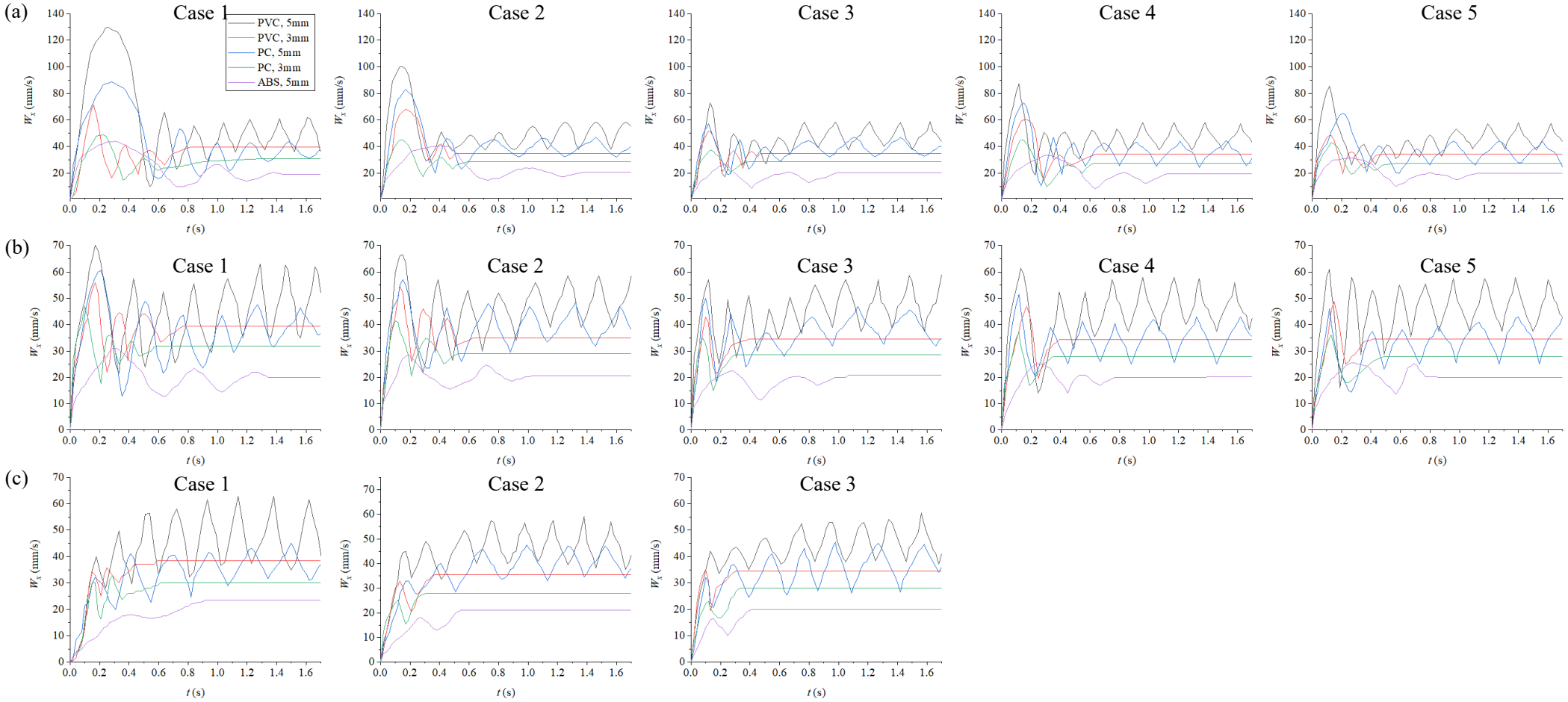


**Figure 3.6** Time evolution of instantaneous vertical settling velocity $W_x$ for MP disks with release angle of (a) 90°, (b) 45° and (c) 0°. MP disks with the release angle of 90° and 45° have five different release ways (Case 1 - Case 5); MP disks of each shape with the release angle of 0° have three release ways (Case 1 - Case 3).

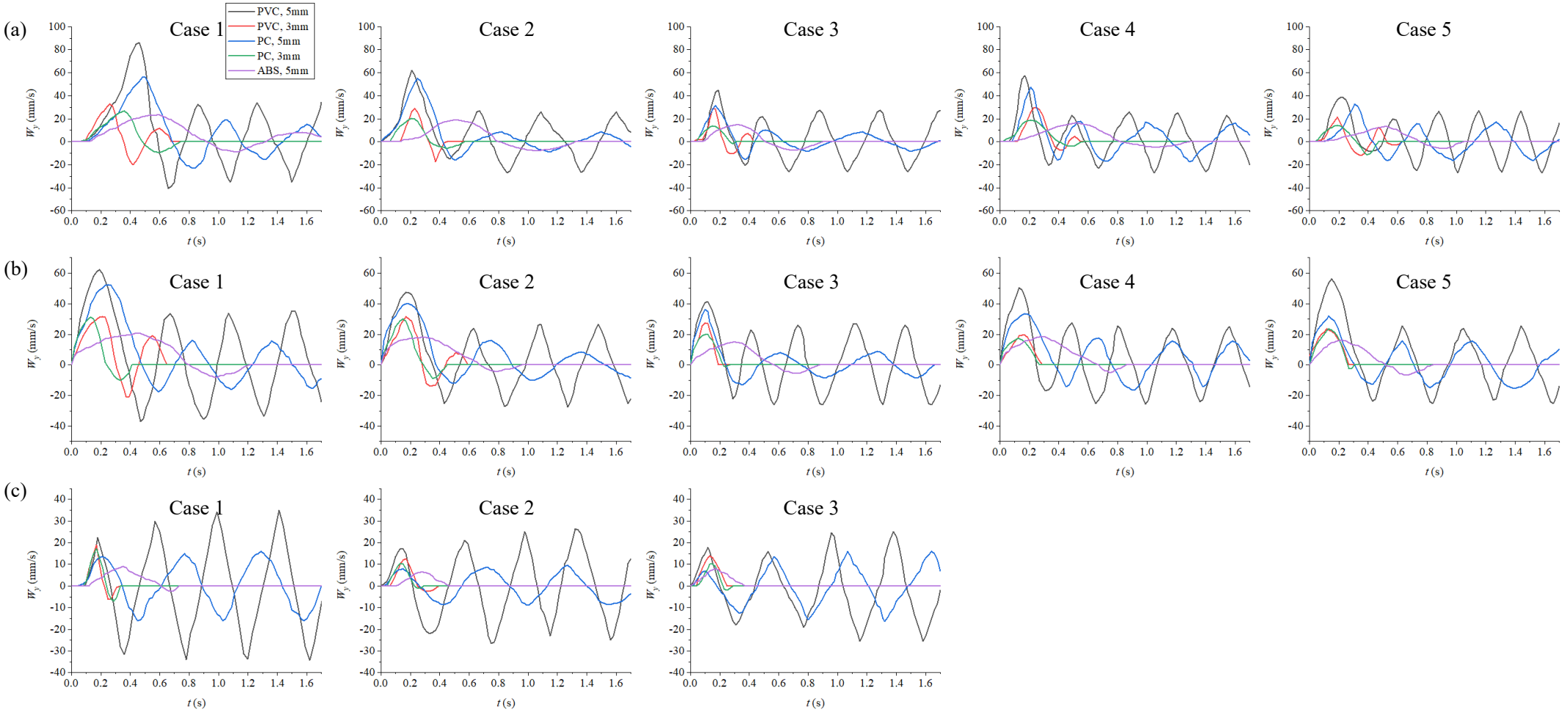


**Figure 3.7** Time evolution of instantaneous horizontal settling velocity $W_y$ for MP disks with release angle of (a) 90°, (b) 45° and (c) 0°.

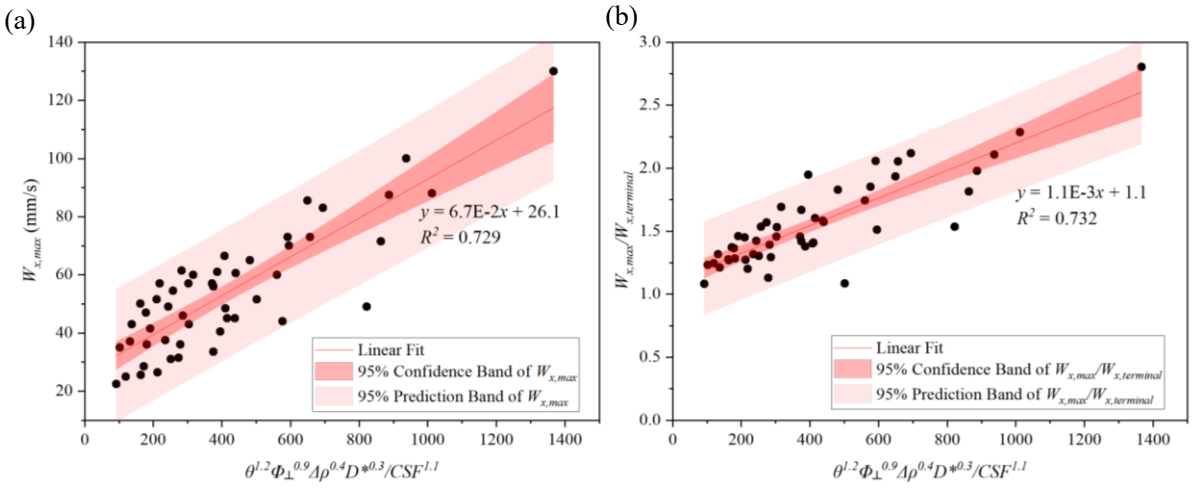


**Figure 3.8** (a) Maximum settling velocity $W_{x,max}$ and (b) ratio of $W_{x,max}$ to mean terminal settling velocity $W_{x,terminal}$ of MP disk in the vertical direction released in five ways (Case 1 - Case 5) with the release angle of 90° and 45°.

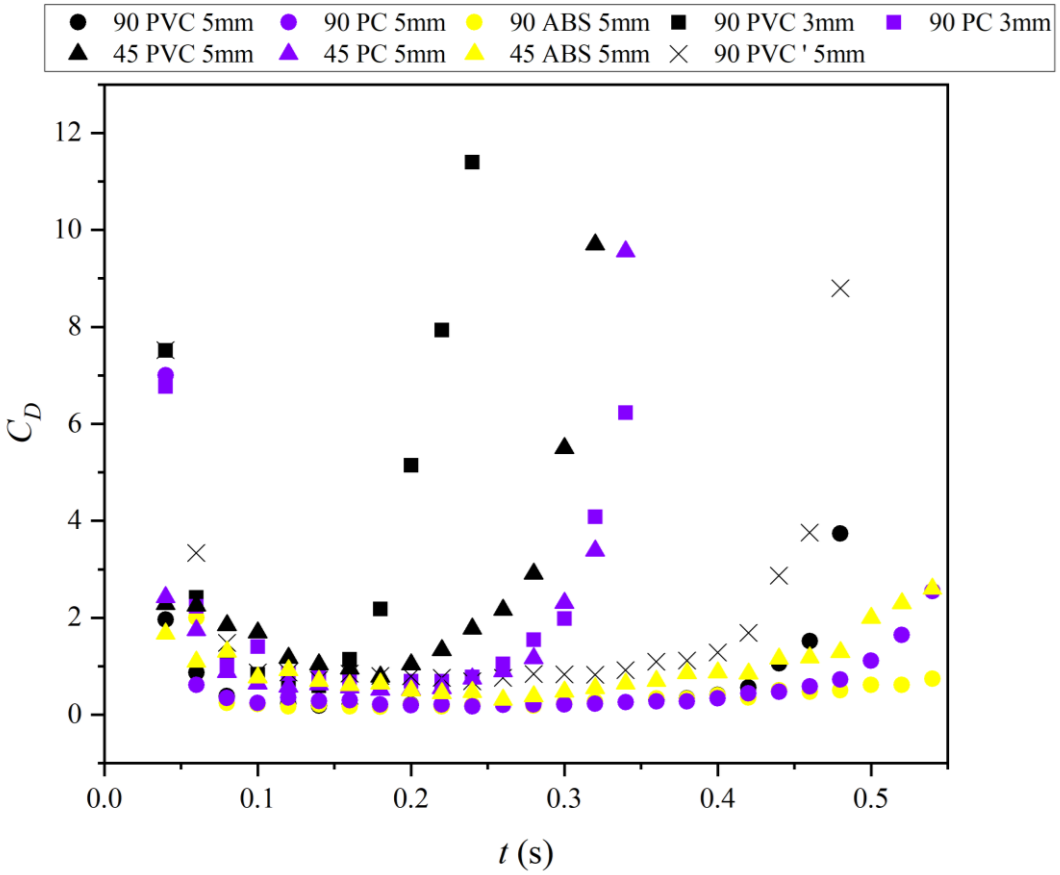


**Figure 3.9** Example of drag coefficient of MP disks in the adjustment phase in Case 1. The size in legend is the side length *l*. The disk in legend with apostrophe (PVC') means $C_D$ calculated by Eqn. (7); others are calculated by Eqn. (6).

# Chapter 4 General Conclusions, Applications and Future Research Directions

## 4.1 General Conclusions

In this research, the settling processes of MP disks before and after reaching their terminal velocities were examined. Due to the significant deviation in shapes, the settling behaviors of MP disks are different from particles of other shapes. Detailed analyses were conducted on the hydrodynamic properties of MP disk settling, including the settling trajectory, settling velocity and drag coefficient. During the settling process, not only vertical falling but also lateral movements was observed. Specific conclusions can be found at the end of Chapter 2 and Chapter 3. The followings are the general conclusions of this research:

1) In the terminal settling phase, three types of settling trajectories of MP disks were identified: MP disks with smaller Reynolds number (< 100) have rectilinear settling trajectory; square disks with larger Reynolds number (> 100) have zigzag settling trajectory; and rectangular and triangular disks with larger Reynolds number (> 100) have zigzag settling trajectory, with the direction of the oscillation rotates from time to time. The settling trajectory is related to the dimensionless moment of inertia and Reynolds number of the disks.

2) In the terminal settling phase, for the MP disks with non-linear settling trajectory, the instantaneous settling velocity in the vertical and horizontal directions, $W_x$ and $W_y$, oscillate periodically. The density and shape of MP impact the frequency, amplitude and extreme (maximum and minimum) values of MP disks. However, the MP disks with rectilinear settling trajectories have consistent instantaneous settling velocity in the horizontal ($W_y = 0$) and vertical ($W_x$ = mean terminal velocity) directions.

3) The mean terminal settling velocity varies according to the density, size and shape of MP disks. The mean terminal settling velocities of MP disks are less than those of MP pellets,

cylinders and fragments. A new dimensionless formula was proposed for the settling velocities of both MP and non-MP disks, which shows a good accuracy with $R^2$ = 0.90 and *Err* = 15.5%.

4) In the terminal settling phase, although the $C_D$ - *Re* equations for spheres underestimate drag coefficient for MP and non-MP disks, the universal $C_D$ - *Re* equation that takes into account the effects of shape and settling orientation exhibits reasonable accuracy for MP disks with *Err* = – 1.71%.

5) The release angles and release ways of same shaped MP disks do not affect the settling trajectory and velocity in the terminal settling phase, but exert substantial impacts in the acceleration phase right after the release. The density, size and shape of MP disks have an influence on the settling trajectory and velocity both in the acceleration and terminal settling phases.

6) In the acceleration phase, the MP disks with a release angle of 0° begin to zigzag immediately after the release and the settling velocity grows gradually. The MP disks with release angles of 45° and 90° initially adjust to the horizontal position before beginning to zigzag. During this adjustment, the settling velocity experience a sharp increase, then decreases after reaching the maximum vertical settling velocity ($W_{x,max}$).

7) In the acceleration phase, the density, size, release angle, *CSF* and crosswise sphericity of MP disks determine the adjustment distances in the vertical ($L_x$) and horizontal ($L_y$) directions as well as the maximum vertical settling velocity ($W_{x,max}$). Quantitative relationships were developed for these parameters with good accuracies.

8) In the adjustment phase, the drag coefficient of MP disks changes with time. The equation of the drag coefficient of accelerating disks was derived. The drag coefficient decreases to the lowest value and then increases, and it is related to density, size and release angle

of MP disks.

## 4.2 Applications

The research results from this study can be potentially applied in the following areas.

1) The equations for settling velocity and drag coefficient can be applied to model MP transport and fate in the environments (rivers, lakes, oceans, stormwater ponds, wetlands, etc.). Based on the modeling results, we can better know or predict the accumulation location of MPs so that we can remove MPs, guide the field sampling of MPs and evaluate the impact of MP pollution to the environments.

2) The equations for the adjustment distance and maximum settling velocity in acceleration process can be applied in understanding MP transport in shallow water (urban street flow, shallow wetlands, swamps, etc.). The urban street flow is the sheet flow during storm events or due to snowmelt, and the acceleration process provides the basic knowledge for MP transport in sheet flow. Besides, in shallow wetlands and swamps, the MP transport in the acceleration phase is also not supposed to be neglected. The results can be used to provide better prediction for MPs distribution and accumulation areas in shallow wetlands and swamps, which is helpful for collection and removal MPs.

3) The settling trajectory and velocity of MPs can be applied to the treatment/removal of MPs in waste water treatment plants (WWTPs). For example, they can be used to examine the existing reactors (e.g., settling tanks). The shapes, density and size of MPs can affect the settling velocity and settling time, which further influence the removal efficiency of different MPs. Thus, the results from this study might be useful for new designs or modification to existing designs in WWTP components to remove MPs from wastewater.

4) The methods and results of this thesis lay a good foundation for studying: (1) MP films, which is thinner than disks and have flexibility in materials, indicating they might have

more complicated settling behaviors; (2) MP fragments, which are close to disks but with irregular shapes; (3) Sub-millimeter MP disks, films and fragments.

### 4.3 Future Research Directions

Based on the literature and this research on MPs, future research could give the priority to:

1) The settling process of sub-millimeter MPs including MP disks. MPs that are smaller than 1 mm exist in environment but the settling process of them is poorly understood. The settling behaviors of sub-millimeter MP fragments has been recently studied (Kaiser, *et al*. 2019), but for MPs of other shapes including spheres, disks and fibers, their settling behaviors are not clear. These investigations help to evaluate the potential transport pathways of small MPs.

2) The acceleration phase of MPs of other shape such as fibers and irregular fragments. These MPs would probably have different accelerating behaviors from MP disks, and understanding these unsteady motions will improve the prediction on the transport and fate of MPs, especially in shallow waters.

3) The settling behaviors of MPs incorporated with other substances. Due to the physical property of MPs, they can absorb other contaminants in surrounding water, which would change the settling behaviors of MPs. In particular, the investigation of MPs with biofilms, heavy metals or organic pollutants is imperative as it gives a close-to-nature understanding on settling behaviors of MPs. So far, only few recent studies (e.g., Semcesen and Wells, 2021; Jalon-Rojas et al., 2022) have examined MPs with biofilms, which showed that biofilms can decrease or increase the settling velocity of MPs. The effects of other pollutions on settling behaviors of MPs are still unknown.

4) The settling behavior of MPs after weathering processes (e.g., due to abrasion and UV light). The weathering processes affect MP physical properties including size, surface

roughness and structural change (Kowalski *et al.*, 2016), which might have an important influence on the settling behaviors. Whether the weathering can affect the settling behaviors needs further investigations.

5) Combination of settling process and other hydraulic processes (e.g., resuspension, incipient motion and bedload). In the real aquatic environment, the settling behaviors of MPs are more complicated than those in stagnant water. To have an accurate prediction of the transport pathway of MPs, studies on the interaction of different motions are needed.

6) Numerical modeling on the settling and other transport means of MPs. Given fundamental experimental studies of MPs, numerical models could be built to have a better understanding of the mechanisms of MP transport behaviors including settling of MP disks. Large-scale modeling can provide the prediction of transport pathways of MPs in the aquatic environment (Ballent *et al.*, 2013; Daily and Hoffman, 2020), based on which mitigation measures can be taken.

**References**

Akanyange, S. N., Lyu, X., Zhao, X., Li, X., Zhang, Y., Crittenden, J. C., . . . Zhao, H. (2021). Does microplastic really represent a threat? A review of the atmospheric contamination sources and potential impacts. *Science of the Total Environment, 777*, 146020.

Alimi, O. S., Farner Budarz, J., Hernandez, L. M., & Tufenkji, N. (2018). Microplastics and Nanoplastics in Aquatic Environments: Aggregation, Deposition, and Enhanced Contaminant Transport. *Environmental Science & Technology, 52*(4), 1704-1724.

Andrady, A. L. (2011). Microplastics in the marine environment. *Marine Pollution Bulletin, 62*(8), 1596-1605.

Andrady, A. L. (2017). The plastic in microplastics: A review. *Marine Pollution Bulletin, 119*(1), 12-22.

Auguste, F., Magnaudet, J., & Fabre, D. (2013). Falling styles of disks. *Journal of Fluid Mechanics, 719*, 388-405.

Bagaev, A., Mizyuk, A., Khatmullina, L., Isachenko, I., & Chubarenko, I. (2017). Anthropogenic fibres in the Baltic Sea water column: Field data, laboratory and numerical testing of their motion. *Science of the Total Environment, 599-600*, 560-571.

Ballent, A., Pando, S., Purser, A., Juliano, M. F., & Thomsen, L. (2013). Modelled transport of benthic marine microplastic pollution in the Nazaré Canyon. *Biogeosciences, 10*(12), 7957-7970.

Ballent, A., Purser, A., de Jesus Mendes, P., Pando, S., & Thomsen, L. (2012). Physical transport properties of marine microplastic pollution. *Biogeosciences Discussions, 9*(12), 18755-18798.

Barnes, D. K., Galgani, F., Thompson, R. C., & Barlaz, M. (2009). Accumulation and fragmentation of plastic debris in global environments. *Philosophical transactions of the royal society B: biological sciences, 364*(1526), 1985-1998.

Camenen, B. (2007). Simple and General Formula for the Settling Velocity of Particles. *Journal of Hydraulic Engineering, 133*(2), 229-233.

Carbery, M., O'Connor, W., & Palanisami, T. (2018). Trophic transfer of microplastics and mixed contaminants in the marine food web and implications for human health. *Environment International, 115*, 400-409.

Cheng, N. S. (2009). Comparison of formulas for drag coefficient and settling velocity of spherical particles. *Powder Technology, 189*(3), 395-398.

Choi, C. E., Zhang, J., & Liang, Z. (2022). Towards realistic predictions of microplastic fiber transport in aquatic environments: Secondary motions. *Water Research, 218*, 118476.

Chubarenko, I., Bagaev, A., Zobkov, M., & Esiukova, E. (2016). On some physical and dynamical properties of microplastic particles in marine environment. *Marine Pollution*

*Bulletin, 108*(1-2), 105-112.

Clift, R., & Gauvin, W. H. (1971). Motion of Entrained Particles in Gas Streams. *Journal of Chemical Engineering, 49*(4), 439-448.

Corey, A. T. (1949). Influence of Shape on the Fall Velocity of Sand Grains. *A&M College, Colorado.*

Daily, J., & Hoffman, M. J. (2020). Modeling the three-dimensional transport and distribution of multiple microplastic polymer types in Lake Erie. *Marine pollution bulletin*, 154, 111024.

Dietrich, W. E. (1982). Settling velocity of natural particles. *Water Resources Research, 18*, 1615-1626.

Dioguardi, F., Mele, D., & Dellino, P. (2018). A New One-Equation Model of Fluid Drag for Irregularly Shaped Particles Valid Over a Wide Range of Reynolds Number. *Journal of Geophysical Research: Solid Earth, 123*(1), 144-156.

Eriksen, M., Lebreton, L. C., Carson, H. S., Thiel, M., Moore, C. J., Borerro, J. C., . . . Reisser, J. (2014). Plastic Pollution in the World's Oceans: More than 5 Trillion Plastic Pieces Weighing over 250,000 Tons Afloat at Sea. *PLoS One, 9*(12), e111913.

Esiukova, E. (2017). Plastic pollution on the Baltic beaches of Kaliningrad region, Russia. *Marine Pollution Bulletin, 114*(2), 1072-1080.

Ferguson, R. I., & Church, M. (2004). A simple universal equation for grain settling velocity. *Journal of Sedimentary Research, 74*, 933-937.

Ferreira, J. M., & Chhabra, R. P. (1998). Accelerating motion of a vertically falling sphere in incompressible. *Powder Technology, 97*, 6-15.

Field, S. B., Klaus, M., & Moore, M. G. (1997). Chaotic dynamics of falling disks. *Nature (London), 388*, 252-254.

Francalanci, S., Paris, E., & Solari, L. (2021). On the prediction of settling velocity for plastic

particles of different shapes. *Environmental Pollution, 290*, 118068.

Free, C. M., Jensen, O. P., Mason, S. A., Eriksen, M., Williamson, N. J., & Boldgiv, B. (2014). High-levels of microplastic pollution in a large, remote, mountain lake. *Marine Pollution Bulletin, 85*(1), 156-163.

Geyer, R., Jambeck, J. R., & Law, K. L. (2017). Production, use, and fate of all plastics ever made. *Science Advances*, 3(7), e1700782

Ghosh, S. K., Pal, S., & Ray, S. (2013). Study of microbes having potentiality for biodegradation of plastics. *Environmental Science and Pollution Research, 20*(7), 4339-4355.

Guo, X., & Wang, J. (2019). The chemical behaviors of microplastics in marine environment: A review. *Marine Pollution Bulletin, 142*, 1-14.

Haider, A., & Levenspiel, O. (1989). Drag Coefficient and Terminal Velocity of Spherical and Nonspherical Particles. *Powder Technology, 58*(1), 63-70.

Hazzab, A., Terfous, A., & Ghenaim, A. (2008). Measurement and modeling of the settling velocity of isometric particles. *Powder Technology, 184*(1), 105-113.

Hidalgo-Ruz, V., Gutow, L., Thompson, R. C., & Thiel, M. (2012). Microplastics in the marine environment: a review of the methods used for identification and quantification. *Environmental Science & Technology, 46*(6), 3060-3075.

Hoerner, S. F. (1965). *Fluid-dynamics drag: Hoerner Fluid Dynamics.*

Hölzer, A., & Sommerfeld, M. (2008). New simple correlation formula for the drag coefficient of non-spherical particles. *Powder Technology, 184*(3), 361-365.

Horton, A. A., & Dixon, S. J. (2017). Microplastics: An introduction to environmental transport processes. *Wiley Interdisciplinary Reviews: Water, 5*(2).

ISO1183-1. (2012). Plastics – Methods for Determining the Density of Noncellular Plastics – Part 1: Immersion Method, Liquid Pyknometer Method and Titration Method. 1-17.

Jalaal, M., Ganji, D. D., & Ahmadi, G. (2010). Analytical investigation on acceleration motion of a vertically falling spherical particle in incompressible Newtonian media. *Advanced Powder Technology, 21*(3), 298-304.

Jalaal, M., Ganji, D. D., & Ahmadi, G. (2012). An analytical study on settling of non-spherical particles. *Asia-Pacific Journal of Chemical Engineering, 7*(1), 63-72.

Jalon-Rojas, I., Romero-Ramirez, A., Fauquembergue, K., Rossignol, L., Cachot, J., Sous, D., & Morin, B. (2022). Effects of Biofilms and Particle Physical Properties on the Rising and Settling Velocities of Microplastic Fibers and Sheets. *Environmental Science & Technology, 56*, 8114-8123.

Kaiser, D., Estelmann, A., Kowalski, N., Glockzin, M., & Waniek, J. J. (2019). Sinking velocity of sub-millimeter microplastic. *Marine Pollution Bulletin, 139*, 214-220.

Khatmullina, L., & Chubarenko, I. (2019). Transport of marine microplastic particles: why is it so difficult to predict? *Anthropocene Coasts, 2*(1), 293-305.

Khatmullina, L., & Isachenko, I. (2017). Settling velocity of microplastic particles of regular shapes. *Marine Pollution Bulletin, 114*(2), 871-880.

Komar, P. D., & Reimers, C. E. (1978). Grain shape effects on settling rates. *The Journal of Geology, 86*(2), 193-209.

Kowalski, N., Reichardt, A. M., & Waniek, J. J. (2016). Sinking rates of microplastics and potential implications of their alteration by physical, biological, and chemical factors. *Marine Pollution Bulletin, 109*(1), 310-319.

Li, L., & Michaelides, E. E. (1992). The magnitude of Basset forces in unsteady multiphase flow computations. *Journal of Fluids Engineering, 114*, 417-419.

Li, W. C., Tse, H. F., & Fok, L. (2016). Plastic waste in the marine environment: A review of sources, occurrence and effects. *Science of the Total Environment, 566-567*, 333-349.

Ma, B., Xue, W., Ding, Y., Hu, C., Liu, H., & Qu, J. (2019). Removal characteristics of

microplastics by Fe-based coagulants during drinking water treatment. *Journal of Environmental Sciences, 78*, 267-275.

Mrokowska, M. M. (2020). Influence of pycnocline on settling behaviour of non-spherical particle and wake evolution. *Scientific reports, 10*(1), 20595.

Obbard, R. W., Sadri, S., Wong, Y. Q., Khitun, A. A., Baker, I., & Thompson, R. C. (2014). Global warming releases microplastic legacy frozen in Arctic Sea ice. *Earth's Future, 2*(6), 315-320.

Ostle, C., Thompson, R. C., Broughton, D., Gregory, L., Wootton, M., & Johns, D. G. (2019). The rise in ocean plastics evidenced from a 60-year time series. *Nature Communications, 10*(1), 1622.

Padervand, M., Lichtfouse, E., Robert, D., & Wang, C. (2020). Removal of microplastics from the environment. A review. *Environmental Chemistry Letters, 18*(3), 807-828.

Roy, N., Wijaya, K. P., Götz, T., & Sundar, S. (2022). Transport of ellipsoidal microplastic particles in a 3D lid-driven cavity under size and aspect ratio variation. *Applied Mathematics and Computation, 413*.

Semcesen, P. O., & Wells, M. G. (2021). Biofilm growth on buoyant microplastics leads to changes in settling rates: Implications for microplastic retention in the Great Lakes. *Marine Pollution Bulletin*, 170, 112573.

Song, X., Xu, Z., Li, G., Pang, Z., & Zhu, Z. (2017). A new model for predicting drag coefficient and settling velocity of spherical and non-spherical particle in Newtonian fluid. *Powder Technology, 321*, 242-250.

Song, Z., Wu, T., Xu, F., & Li, R. (2008). A simple formula for predicting settling velocity of sediment particles. *Water Science and Engineering, 1*(1), 37-43.

Stringham, G. E., Simons, D. B., & Guy, H. P. (1969). The behavior of large particles falling in quiescent liquids. US Government Printing Office, 562-c.

Torabi, M., & Yaghoobi, H. (2011). Novel solution for acceleration motion of a vertically falling spherical particle by HPM–Padé approximant. *Advanced Powder Technology, 22*(5), 674-677.

Van Melkebeke, M., Janssen, C., & De Meester, S. (2020). Characteristics and Sinking Behavior of Typical Microplastics Including the Potential Effect of Biofouling: Implications for Remediation. *Environmental Science & Technology, 54*(14), 8668-8680.

Waldschläger, K., & Schüttrumpf, H. (2019). Effects of Particle Properties on the Settling and Rise Velocities of Microplastics in Freshwater under Laboratory Conditions. *Environmental Science & Technology, 53*(4), 1958-1966.

Wang, Y., Shu, C., Teo, C. J., & Yang, L. M. (2016). Numerical study on the freely falling plate: Effects of density ratio and thickness-to-length ratio. *Physics of Fluids, 28*(10).

Wang, Y., Zhou, L., Wu, Y., & Yang, Q. (2018). New simple correlation formula for the drag coefficient of calcareous sand particles of highly irregular shape. *Powder Technology, 326*, 379-392.

Willmarth, W. W., Hawk, N. E., & Harvey, R. L. (1964). Steady and Unsteady Motions and Wakes of Freely Falling Disks. *Physics of Fluids, 7*(2).

Yaghoobi, H., & Torabi, M. (2012). Novel solution for acceleration motion of a vertically falling non-spherical particle by VIM–Padé approximant. *Powder Technology, 215-216*, 206-209.

Yang, D., Shi, H., Li, L., Li, J., Jabeen, K., & Kolandhasamy, P. (2015). Microplastic Pollution in Table Salts from China. *Environmental Science & Technology, 49*(22), 13622-13627.

Yin, Z., Wang, Z., Liang, B., & Zhang, L. (2017). Initial Velocity Effect on Acceleration Fall of a Spherical Particle through Still Fluid. *Mathematical Problems in Engineering, 2017*, 1-8.

Yonkos, L. T., Friedel, E. A., Perez-Reyes, A. C., Ghosal, S., & Arthur, C. D. (2014). Microplastics in four estuarine rivers in the Chesapeake Bay, U.S.A. *Environmental Science & Technology, 48*(24), 14195-14202.

Yu, Z., Yang, G., & Zhang, W. (2022). A new model for the terminal settling velocity of microplastics. *Marine Pollution Bulletin, 176*, 113449.

Zastawny, M., Mallouppas, G., Zhao, F., & van Wachem, B. (2012). Derivation of drag and lift force and torque coefficients for non-spherical particles in flows. *International Journal of Multiphase Flow, 39*, 227-239.

Zhang, H. (2017). Transport of microplastics in coastal seas. *Estuarine, Coastal and Shelf Science, 199*, 74-86.

Zhao, S., Wang, T., Zhu, L., Xu, P., Wang, X., Gao, L., & Li, D. (2019). Analysis of suspended microplastics in the Changjiang Estuary: Implications for riverine plastic load to the ocean. *Water Research, 161*, 560-569.

Zhong, H., Chen, S., & Lee, C. (2011). Experimental study of freely falling thin disks: Transition from planar zigzag to spiral. *Physics of Fluids, 23*(011702).

Zhong, H., Lee, C., Su, Z., Chen, S., Zhou, M., & Wu, J. (2013). Experimental investigation of freely falling thin disks. Part 1. The flow structures and Reynolds number effects on the zigzag motion. *Journal of Fluid Mechanics, 716*, 228-250.